QUANTUM DOT SENSITIZED

ZNO NANOWIRE-P3HT HYBRID

PHOTOVOLTAICS

by

NICHOLAS ANDREW HARRIS

PATRICK KUNG, COMMITTEE CHAIR

SEONGSIN KIM
DAVID NIKLES

A THESIS

Submitted in partial fulfillment of the requirements
for the degree of Master of Science
in the Department of Electrical Engineering
in the Graduate School of
The University of Alabama

TUSCALOOSA, ALABAMA

2012

ABSTRACT

A hybrid, nanostructured solar cell architecture has been designed, described, fabricated and characterized. ZnO nanowires were synthesized using thermal chemical vapor deposition to act as a high energy photon absorber scaffold and electron transport pathway. InP-ZnS core-shell quantum dots were attached to the nanowires via surface chemistry to act as a high-efficiency sensitizing absorption medium. A ligand exchange procedure was performed to cap the quantum dots with mercaptopropionic acid for improved adhesion to ZnO nanowires and improved electrical properties. Experimentation was performed to optimize the surface chemistry adhesion of the ligand exchange and quantum dot-nanowire adhesion. A thoroughly-filled P3HT matrix was drop coated selectively and annealed into the quantum dot sensitized nanowire array to serve as a hole capture and transport, absorption, and planarizing medium. Characterization was performed throughout device fabrication using SEM, TEM, XRD, PL spectroscopy, Raman spectroscopy, UV-Vis spectroscopy, and electrical measurements. A dense monolayer of quantum dots was deposited and imaged via HRTEM. PL quenching of quantum dots in P3HT was observed. The viability and advantages of quantum dot sensitization of a hybrid ZnO nanowire-P3HT hybrid were shown via PL, UV-Vis and device electrical measurements.

DEDICATION

This thesis is dedicated to Jesus Christ.

ACKNOWLEDGMENTS

I would like to thank all of my family, friends and advisors for all of the support and knowledge shared with me throughout this research project. I thank God for his provision, strength, wisdom and steadfast love. I thank the sponsors of the fellowships provided to me while working on this thesis. My co-workers, who are all friends, have provided physical, moral and intellectual support all throughout this process, without which, this project would have never made any meaningful progress. My family members have all sacrificed in one way or another to help provide for me the chance to pursue my education further. My friends have supported me and uplifted me whenever I have lost confidence. My advisors have given me professional direction. I thank all those who have given of themselves to help make this possible for me. Thank you.

CONTENTS

LIST OF FIGURES

LIST OF ILLUSTRATIONS

CHAPTER 1

INTRODUCTION

Quantum dot (QD) functionalized nanostructures and hybrid organic/inorganic photovoltaic devices have attracted considerable attention in recent years due to the potential for low cost and low temperature processing of the materials [1-3]. QDs have the potential for increased stability and lifetime compared to traditional dyes and also have the potential for multiple electron generation per photon [4-8] as well as an absorption spectrum that can be tuned via quantum dot size [8]. Core-shell quantum dots have been shown to offer a more stable structure than single material quantum dots without a capping layer [9]. Nanowire scaffolds have been extensively used as efficient, low resistance electron transport pathways which minimize the hopping mechanism in the charge transport process of quantum dot solar cells [1-4,9]. Single crystal high bandgap semiconductor nanowires can, in addition to providing an efficient electrical transport medium, act as an additional photon absorbing material for short wavelength photons, both generating near bandgap excitons and providing a protective structure for the rest of the architecture from caustic UV radiation. However, the use of liquid electrolytes within these scaffold device structures, such as triiodide/iodide, as a hole transport medium has led to significant degradation of the QDs [4].

The device structure was designed to combine the best ideas of several different structures. Quantum dot array solar cells have excellent absorption properties, capable of tuning

the band gaps of the comprising quantum dots by altering the quantum dot size, allowing a more efficient capture of the energy within the solar spectrum by absorbing incident photons at or near their respective energy values and allowing even the capture of low energy, high wavelength photons that are outside the range of traditional silicon solar cells. This benefit alone is key, opening up a larger portion of the solar spectrum as harvestable energy, thus opening up the possibility for devices capable of surpassing the Shockley-Queisser limit [10]. However, the carrier dynamics of such structures are often poor, specifically free carrier pair recombination, due to the interfacial hopping mechanism of free carriers within the arrays of quantum dots and the poor p-n junction characteristics offered by such structures [8, 11, 12]. Polymer based bulk heterojunction solar cells have the advantages of simple and inexpensive manufacture and abundant materials, as well as relatively long free carrier lifetimes. However, such architectures often have even longer transit times, leading to a relatively large loss from the already meager numbers of generated free carriers caused by non-ideal absorption spectra [13]. Quantum dots interspersed throughout such polymer bulk heterojunction solar cell architectures offer a simple method to improve absorption properties, specifically offering the capability of multiple exciton generation, and might even slightly improve carrier dynamics while the polymer matrix protects the quantum dots from deterioration; however, long transit times are still a problem that plagues such solar cells. Lastly, the device structure of single-crystal nanowires submerged in a liquid or polymer matrix offers better carrier dynamics, as well as low manufacture costs, but still presents the problem of an absorption spectrum that is not capable of efficiently capturing the full range of photon energies found in the solar spectrum [13, 14]. The focus of this project has been a quantum dot sensitized hybrid ZnO nanowire/P3HT solar cell. The goal of the project was to take steps towards producing a high efficiency, low cost solar cell that makes use of inexpensive

manufacture processes and abundant materials. In doing so, several growth and deposition methods, typical methods of characterization, and the relevant surface chemistry and physics of device operation of quantum dots secondarily and solar cells primarily have been utilized.

By attaching quantum dots to a scaffold of nanowires and depositing a matrix onto the nanowires and dots, the advantages offered by each of the above architectures can be utilized in order to produce a low-cost and high-efficiency solar cell. The quantum dots allow for near-band-gap capture of photons by varying quantum dot size and thus band gap to prevent loss of energy due to "hot carriers" or above band gap excitons relaxing to a lower energy state at the bottom of the conduction band prior to electron-hole pair separation through the generation of phonons. The discrete energy levels afforded by quantum dots also aid in preventing the loss of energy due to hot carrier cooling. This phenomenon actually opens up the possibility of generating multiple excitons from a single high-energy photon if the initial high energy exciton can be separated into free carriers prior to relaxation; this requires surface contact with a fast electron donor or acceptor material, often referred to as an electron or hole trap. The single-crystal nanowire scaffold offers a pathway for efficient carrier transit, avoiding interfacial hopping. By attaching quantum dots directly to the nanowires, the design of the device structure attempts to optimize the transitional properties of the free carriers generated in the quantum dots. The polymer matrix is chosen to act as an efficient capture and transfer medium for holes, completing the requisite p-n junction of the device. The polymer encases and protects the quantum dots from deterioration and accepts the opposite free carrier of the nanowires. This hybrid device structure attempts to maximize the benefits of several different architectures in order to optimize device performance while minimizing the need for expensive processing techniques. A graphic model of the described architecture may be found in Illustration 1.1.

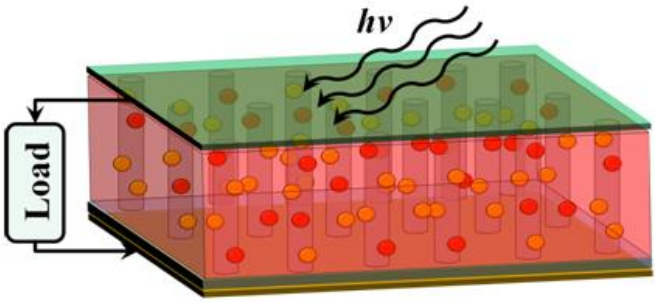

Illustration 1.1 Sketch of device structure.
The top layer is a transparent conducting substrate onto which nanowires are grown. The middle layer is comprised of a quantum dot functionalized nanowire scaffold embedded in a polymer matrix. The bottom layer consists of a contact attached to the bottom of the polymer.

CHAPTER 2

CHARACTERIZATIONS

Several different types of characterization have been performed to assess the quality and performance of the devices at several steps throughout processing. Photoluminescence spectroscopy (PL) was utilized to gauge the number of defects in the nanowires and as a quantification for attached quantum dots. The confocal PL measurements for this work were carried out utilizing a Princeton Instruments Monovista spectroscopy system using either a Coherent Verdi V-12 532 nm wavelength laser or MBD-266 UV laser serving as the excitation source. Confocal microscopy refers to the use of a focusing objective to focus illumination to a specific area on a specimen, as opposed to broad or unfocused illumination, and to filter the reflected illumination, along with the emitted signal passing through an aperture, of all photons not originating from within the selected area. By incorporating a microscope into the PL measurement setup, enhanced spatial resolution was attained. Several filters are available for reducing laser intensity incident upon the specimen. The spectrometer for this setup had three different gratings (1200, 1800, and 2400 groove/mm) which were used to spatially disperse the incident light by wavelength which is then directed onto a charge-coupled device (CCD) for detection. The angle of the grating was rotated while instantaneous snapshots were taken with the CCD. These frames were then superimposed to form an entire spectrum from the snapshots. Nanowire and P3HT samples were used as-grown/-deposited on substrate for PL spectroscopy. However, higher energy and intensity laser excitation has been linked to a loss of detected

photons luminesced from quantum dots; therefore, energy, intensity, and exposure was minimized for quantum dot functionalized samples.

Raman spectroscopy was used to verify molecular composition. Standing wave crystal lattice vibrational modes offer another mechanism through which light interacts, producing Raman scattering, by which materials may be characterized. The same setup as used for the confocal PL measurements was also used to perform the confocal Raman spectroscopy measurements for this work; however, solely the Verdi 532 nm wavelength laser was used as the excitation source. Nanowire samples were used as-grown on substrate for Raman spectroscopy.

Transmission electron microscopy (TEM) was used to take high resolution images that depict the orientation and size of the nanowires and the quantum dot coverage of the nanowires. TEM measurements were performed using an FEI Tecnai F-20 using a small spot size beam accelerated at 200 kV. The TEM was also equipped with a charged-couple device (CCD) camera for scanning transmission electron microscopy (STEM) imaging and an Oxford EDAX energy dispersive spectroscopy (EDS) used for chemical mapping. Preparation of samples for TEM analysis required a single nanowire be isolated and deposited on a pre-fabricated TEM 200 mesh copper grid. An as-grown nanowire on substrate sample was submerged in a 3 mL ethanol solution and sonicated for approximately 20 seconds. A single drop of the solution was then deposited onto the mesh grid. This grid was then mounted onto a double tilt holder used for TEM analysis.

EDS via TEM was used to determine what and where elements were present on quantum dot functionalized nanowire samples. STEM is a mode of operation on the TEM equipment that allows the functionality of an SEM under TEM conditions. In conventional TEM, the electron beam travels through the sample and is focused to a fine point past the sample at the back focal

plane. In STEM mode, the beam is focused at the surface of the sample, providing a small probe scanning the sample. This method of operation can be used in conjunction with an EDS detector in order to analytically perform chemical characterization of the sample. When an electron beam interacts with the sample, it may excite an electron in an inner shell, ejecting it from the shell while creating an electron hole where the electron was located. A higher-shell electron then drops to the hole producing a characteristic X-ray. The energy of the X-ray is characteristic of the difference in energy between the two shells and the atomic structure of the element from which they are emitted. This characteristic energy value can be measured by an energy-dispersive spectrometer.

Scanning electron microscopy (SEM) was used to assess the density, thickness, length, and orientation of the nanowires after growth. SEM was used to evaluate the filling of the nanowire scaffold, as well as the roughness of the top of the P3HT layer prior to contact deposition. SEM measurements were performed using a JEOL 7000F Scanning Electron Microscope and a Philips XL-30 Scanning Electron Microscope. The JEOL microscope was equipped with a Schottky field emitter electron gun with a beam operated between 15-20 kV and a chamber pressure of approximately 10^{-5} Pa; the XL-30 was equipped with a filament electron emitter with a beam operated also at 15-20 kV at a chamber pressure on the order of 10^{-5} Pa. A working distance of approximately 10 mm was used, optimizing the available resolution. Nanowire and P3HT samples were used as-grown/-deposited on substrate for scanning electron microscopy. For cross-sectional images of a deposited P3HT matrix within an array of ZnO nanowires, as-deposited samples were cleaved using a razor blade or a diamond-tipped cutting tool.

X-ray diffraction (XRD) was utilized to determine the composition, crystallography, and orientation of the nanowires. XRD was performed using a Philips X'PERT x-ray diffractometer with a copper x-ray source. The Cu $K_{\alpha 1}$ transition energy corresponds to the primary photon wavelength of the beam, $\lambda = 1.54056$ Å; however, the instrument used was not outfitted with a monochromator and a less intense signal of Cu $K_{\alpha 2}$ photon wavelength of $\lambda = 1.54439$ Å was also present in the beam. This caused a dual peak phenomenon. Specimen were first calibrated to the stage of the diffractometer, then a 2θ-Ω scan was performed wherein the stage was rotated through a range of angles with respect to the incident beam and the detector was rotated in synchronization with the stage at twice the angular rate of the stage's rotation to the incident beam. The sample was the center of the axes of rotation. Samples were used as-grown/-deposited on substrate for XRD.

Optical UV-visible spectrum absorption and transmission measurements were performed to determine optical characteristics of nanowire samples all throughout device fabrication. UV-Vis was performed using a Varian Cary 50 Scan spectrophotometer. This spectrophotometer used a Xenon lamp for illumination with a spectral range of 190 nm to 1.1 μm. Samples were used as-grown/-deposited on transparent substrate for UV-Vis spectroscopy. Rough or reflective substrates greatly reduced the intensity of the transmitted beam; an appropriate scaling factor adjustment is applied to UV-Vis spectra performed and reported in this study.

Electrical measurements were utilized to determine device current-voltage characteristics. Two-point probe electrical measurements were taken using a Keithley 2612A sourcemeter with a Semiprobe probe station using Semiprobe MA-8005 manipulators and tungsten probes. Illumination was provided using a Fiber-Lite MI-152 using a quartz halogen lamp; the samples were illuminated through the microscope column of the source meter and the light was focused

through the objective onto a specific area on the surface of the sample. Samples were used as-grown/-deposited or with sputtered Au contacts on non-conducting deposited materials. In order to prevent a Schottky diode effect between the tungsten probes and GaN thin-films on the substrates, GaIn eutectic was used to provide an electrical pathway between Au contact pad and thin-film. When performing electrical measurements on a sample photovoltaic device, illumination was incident upon the reverse side of the device, due to physical constraints. Rough or reflective substrates also greatly reduced the intensity of incident illumination.

CHAPTER 3

MATERIALS

The design has been implemented to minimize the use of toxic, sparse, or expensive to process materials while optimizing device performance. ZnO nanowires are the basis of the device structure, offering a less expensive option than the popular, but expensive ITO nanowires [15]. The nanowires were grown in the c-direction on an epitaxial n-doped wide bandgap semiconductor layer deposited on <001> plane Al_2O_3 substrate using thermal chemical vapor deposition (CVD) via carbo-thermal reduction of ZnO powder in graphite powder under an atmosphere of Argon. ZnO nanowires have shown an excess of free electrons, making it an n-type material, and a good electron transport medium. Experimentation has also been performed on further n-type doping of the nanowires. The well aligned nanowires are a good conductor of electricity, with a conductance on the order of 1-2 $(\Omega\text{-cm})^{-1}$. Nanowires have also been grown on the sapphire substrate with a zinc acetate seed. InP-ZnS core-shell quantum dots are attached in-solution to the nanowires by use of surface chemistry. InP-ZnS core-shell quantum dots are a less toxic alternative to the popular CdSe quantum dots [16-18], allowing for less expensive and safer handling of the quantum dots. The core-shell architecture may also allow for superior charge separation characteristics. Colloidally-grown quantum dots were purchased from NN-Labs, Inc., and stored in solution in toluene. Upon purchase, the quantum dots were capped in an oleylamine ligand. The quantum dots undergo a ligand exchange process in a methanol solution, replacing

the oleylamine with mercaptopropionic acid (MPA), and were then attached to nanowires on a substrate in the methanol solution. Poly (3-hexylthiophene) (P3HT) was drop coated onto the quantum dot functionalized nanowires to coat the wires completely. P3HT is a polymer with good hole-transport properties that can conveniently be dissolved in a solution of trichlorobenzene for ease of deposition via drop or spin coating, minimizing production costs. There has been some experimentation with plasma etching on the P3HT in order to planarize the surface prior to contacts being attached, but currently no etching is being done. Lastly, Au contacts are deposited onto the P3HT to optimize the interface for device testing. Illustration 3.1 depicts the relative energy band levels of the primary materials used in photovoltaic architecture. Bulk energy levels are used. Due to relative energy levels of ZnO and P3HT, P3HT should act as an efficient, fast hole trap whereas ZnO should act as an efficient free electron trap and conductive medium fast transport pathway. ZnS comprises the shell of the core-shell quantum dots.

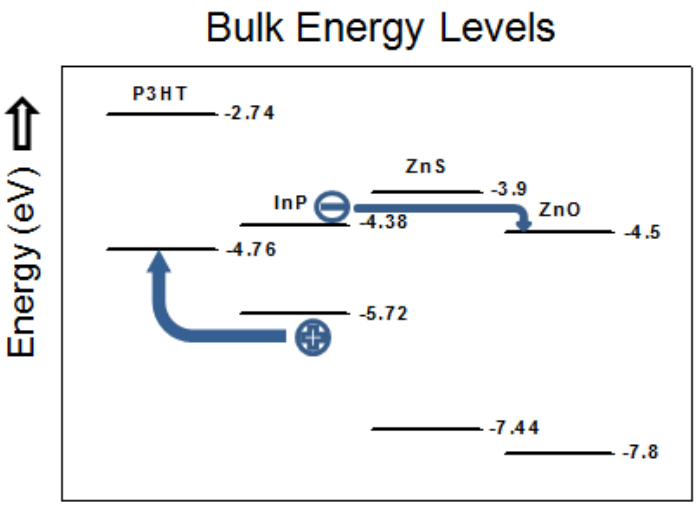

Illustration 3.1 Bulk band level diagram.
Material denoted at head of column. Top line corresponds to conduction band level. Bottom line corresponds to valence band level. Energy value denoted to side of energy level. Energy levels of P3HT representative of electron affinity and effective band gap. GaN thin film layer on substrate used for subsection of samples [19].

A. ZnO Nanowires

ZnO, a II-VI semiconductor, has several unique properties. ZnO has a molar mass of 81.408 g/mol. The wide direct band gap of ZnO of 3.37eV enables it to be a promising material for applications of short wavelength optical devices like UV lasers and light emitting diodes. ZnO normally forms into either hexagonal wurtzite with lattice constants a = 3.25 Å and c = 5.2 Å, cubic zincblende, or rock salt. A large exciton binding energy of 60 meV ensures efficient excitonic emission at room temperature. ZnO has a high electron mobility of 205 $cm^2(V \cdot s)^{-1}$ at room temperature and a peak electron mobility of approximately 2000 $cm^2(V \cdot s)^{-1}$ at 50 K [20]. Besides solar cells, ZnO also has other applications including transparent electronics, chemical and biological sensors, and mechanical energy harvesting devices due to its good transparency, strong room-temperature photoluminescence, high heat capacity, high thermal conductivity, low

thermal expansion, a melting point of 1975° C, and a hardness of 4.5 on the Mohs scale. The well aligned nanowires are a good conductor of electricity, with a conductance on the order of 1-2 $(\Omega\text{-cm})^{-1}$. ZnO is insoluble in water. ZnO is often unintentionally doped n-type, a phenomenon the cause of which is currently under debate. Oxygen vacancies are one considered possibility, while an argument has been made for impurities as well. Due to the unintentional intrinsic doping of ZnO, suitable p-type doping of ZnO remains a challenge. ZnO, as many other materials, displays different properties when sizes are reduced down to nanometer scale. These properties include a high surface to volume ratio and other physical properties arising from quantum confinement. ZnO is probably the richest family of nanostructures among all materials, both in structures and properties. ZnO nanostructures, including nanowires, nanorings, nanobelts, and so on, form the building blocks of many devices such as nanolasers, field-effect transistors, and gas sensors. Several different methods are popular for synthesizing all these different nanostructures. The vapor-liquid-solid method is a sufficient way to grow well-aligned ZnO nanowires using Au or Sn as a catalyst on different kinds of substrate. Other methods, including metal-organic chemical vapor deposition, molecular beam epitaxy and solution growth provide good ZnO nanostructure as well. However, the growth mechanism of ZnO nanostructure remains unclear and the properties of ZnO nanostructure vary from one process to another.

B. InP-ZnS Core-Shell Quantum Dots

Quantum dots are nanostructures of sufficiently small size to exhibit quantum confinement effects in three orthogonal spatial directions. Due to these three-dimensional confinement properties, the size and shape of quantum dots have a strong effect on the electrical and optical properties of the nanostructure. Due to the high degree of control over the size of produced semiconductor nanocrystals, the properties of quantum dots can be easily manipulated.

The band gap is a prime example: in general, as the size of the quantum dot is decreased, the band gap increases, increasing the minimum energy of absorbed photons and the energy of luminesced photons, causing a blue shift in luminescence. Quantum dots exhibit a much less broad density of states than bulk materials or other quantum structures with less dimensions of confinement. Due to their excellent optical and electrical transport properties pertaining to quantized energy spectra and density of states, quantum dots are being used and researched for use in a plethora of applications, including diode lasers, photodetectors, biological and biomedical applications, light emitting devices, and quantum computing. Cadmium- and other heavy metal-free quantum dots are of particular interest due to their potential for use in consumer and commercial devices. There are a variety of methods currently used to produce quantum dots; however, colloidal synthesis is the method used for the fabrication of the quantum dots used in this study.

Colloidally-grown InP-ZnS core-shell quantum dots were purchased from NN-Labs, Inc. Bulk InP is an III-V semiconductor with a direct band gap of 1.344 eV, and forms the core of the core-shell quantum dots. InP most commonly crystallizes in the zincblende structure with a lattice constant of 5.86 Å. InP has a molar mass of 145.792 g/mol. ZnS, an II-VI semiconductor, forms the shell of the quantum dot. ZnS most often crystallizes into either a cubic zincblende structure with a bulk band gap of 3.54 eV, or a hexagonal wurtzite structure with a bulk band gap of 3.91 eV. The cubic zincblende structure of ZnS has a lattice constant of 5.42 Å, whereas the hexagonal wurtzite structure of ZnS has lattice constants of a = 3.82 Å and c = 6.26 Å. ZnS has a molar mass of 97.474 g/mol. The shell of ZnS increases the stability of the quantum dots, but also forms a heterojunction with the InP, enhancing the properties of the quantum dot. Although the junction characteristics differ greatly in the nanostructure regime, bulk InP and ZnS form a

type-I heterojunction. As purchased, the quantum dots were capped with an oleylamine ligand. The quantum dots were stored in a 5 mg/mL concentration solution of toluene. Four sizes of quantum dots were used in this study, represented by the approximate photon wavelength associated with their effective band gaps: 650 nm, 590 nm, 560 nm and 530 nm. These quantum dots range in size from approximately 5 nm to 7 nm in diameter. The size-tunable property of the band gap of quantum dots is evidenced by the varying colors seen in solutions of similar concentration and molecular composition, differing only by the size of the nanocrystals contained within. A figure depicting this phenomenon may be found in the appendix.

Figures 3.1 and 3.2 depict the PL spectra of the 590 nm and 650 nm emission peak quantum dots, respectively, dried from solution onto a glass slide. Confocal PL spectroscopy is performed using a 532 nm laser excitation source. In general, quantum dot emission spectra are expected to be roughly Gaussian in shape. The peak shoulders seen in the figures are therefore unexpected for well-grouped, like-sized quantum dots possessing similar properties. The peak in Figure 3.1 is centered at 623 nm; the peak in Figure 3.2 is centered at 688 nm.

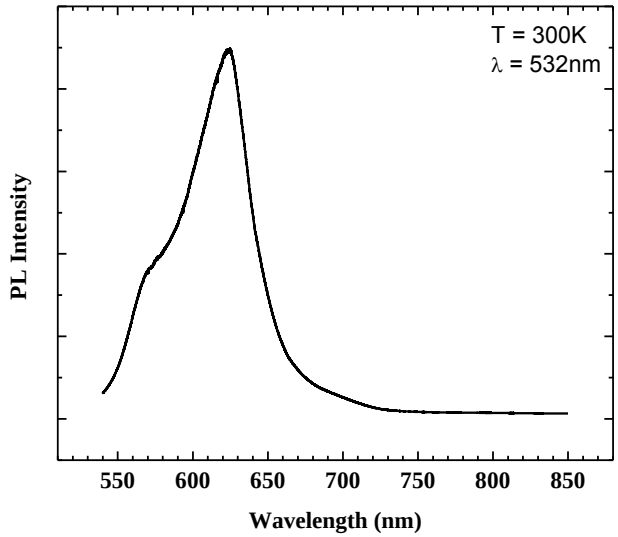

Figure 3.1 PL of 590 nm quantum dots.
Confocal PL spectroscopy scan of InP-ZnS core-shell quantum dots with an expected emission peak at 590 nm on glass slide photoexcited by 532 nm laser.

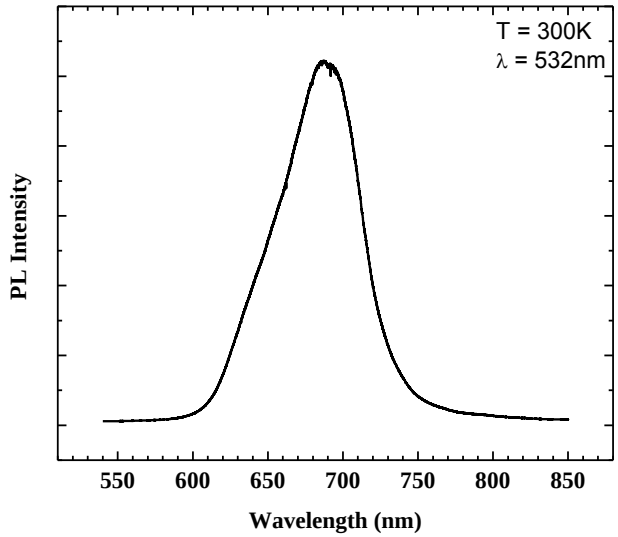

Figure 3.2 PL of 650 nm quantum dots.
Confocal PL spectroscopy scan of InP-ZnS core-shell quantum dots with an expected emission peak at 650 nm on glass slide photoexcited by 532 nm laser.

Figure 3.3 depicts a confocal Raman spectrum for InP-ZnS core-shell quantum dots dried from solution on a glass slide. Peaks can be found at 305 cm^{-1}, 460 cm^{-1}, 629 cm^{-1}, and 980 cm^{-1}; the peak at 305 cm^{-1} corresponds to a transverse optical (TO) phonon mode of InP [21, 22], and can be utilized to characterize the quantum dots.

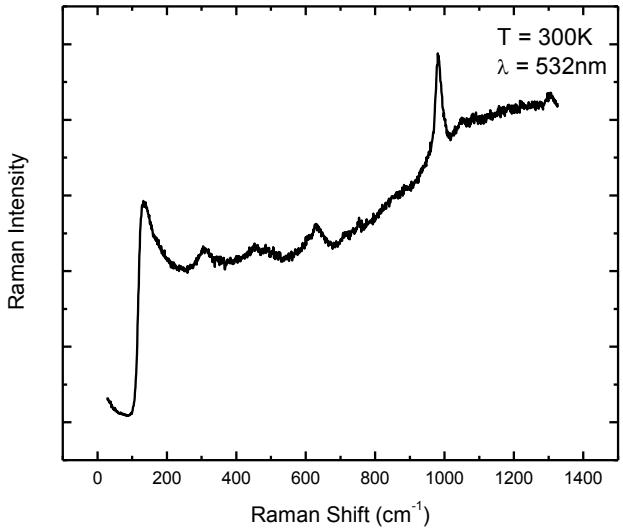

Figure 3.3 Raman of quantum dots.
Confocal Raman spectroscopy scan of InP-ZnS core-shell quantum dots with an expected photo-emission peak at 590 nm on a glass slide photoexcited by 532 nm laser. The spectrum of the glass slide has been removed from the displayed spectrum.

C. Poly(3-hexylthiophene) Polymer Matrix

P3HT was used as the hole-conducting polymer matrix in which the quantum dot functionalized nanowire scaffold is embedded. P3HT is a conductive polymer, with conductivity on the order of 10^{-6} Ω^{-1}-cm^{-1} [23]. P3HT also completes the p-n junction of the device, providing a medium with excess holes in contrast to the inherent unintentional n-type doping of the ZnO nanowires. Regio-regular P3HT, used for its enhanced electrical properties, was purchased from Rieke Metals, Inc. P3HT has a chemical formula of $(C_{10}H_{14}S)_n$. P3HT melts at 238° C. P3HT is soluble in chloroform, trichlorobenzene, chlorobenzene, toluene and xylenes. P3HT is used in many organic solar cell architectures for its excellent hole capture properties, slow recombination rate, and ease of deposition. P3HT has an effective band gap of 2.02 eV, with an electron affinity of 2.74 eV, making it an excellent hole trap medium. Given the widespread use

of P3HT in durable polymer bulk heterojunction architectures [24], as well as the increasing use of dispersed quantum dots in P3HT to enhance the hole transport and power conversion efficiency in hybrid architectures [25-27], P3HT should also provide a less caustic environment for quantum dots than electrolytic liquid hole transport mediums.

Figure 3.4 depicts a UV-Vis transmission spectrum of a P3HT sample. A film of P3HT was deposited onto a sapphire substrate coated with a ZnAlO thin film. The P3HT was drop coated in a solution of trichlorobenzene, allowed to dry, and then annealed. The sizeable drop in transmission at and below approximately 620 nm corresponds to the absorption of P3HT; wavelengths greater than 620 are below the efficient absorption energy range of P3HT. This shows that P3HT is not only effective as a hole capture and transport matrix, but also as an additional layer of effective absorption material. The band edge of the ZnAlO can be seen at approximately 380 nm. The P3HT thickness was measured to be on the order of 1.2 μm. As can be seen, even a thin film of P3HT can act as an effective absorption layer, minimizing required device thickness. This is an important distinction as traditional conjugated polymers often have hole diffusion lengths on the order of 10 nm and absorption lengths on the order of 100 nm [28].

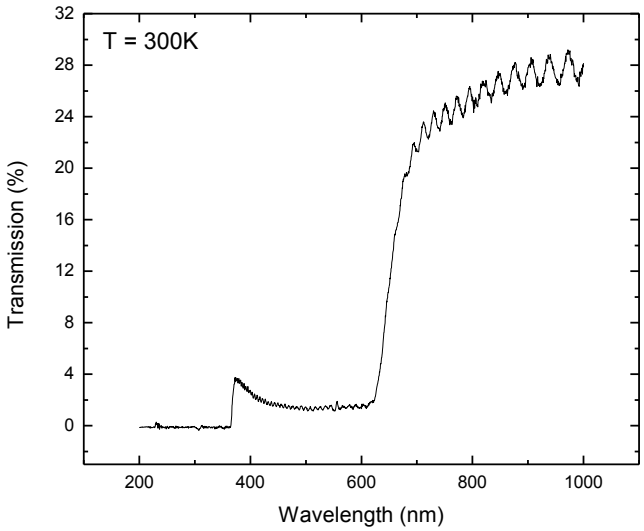

Figure 3.4 Transmission of P3HT.
UV-Vis transmission spectroscopy scan of a P3HT film deposited onto a ZnAlO thin film coating on a sapphire substrate.

CHAPTER 4

FABRICATION

A. Nanowire Synthesis

In this device structure, growth of ZnO nanowires was the first step. Nanowire synthesis was performed using thermal CVD through both catalyst-assisted and catalyst-free method on sapphire <001> substrate plain, coated with aluminum-doped ZnO and coated with GaN. CVD was performed in a tube furnace at 900° C under flow of ultra high purity argon. ZnO powder was evaporated with carbo-thermal reduction in graphite powder using a 1:2 molar ratio. The crystal structure was then verified by XRD and the morphology is studied via SEM. Vibrational properties and optical properties were investigated by Raman spectroscopy and PL. The ZnO nanowires are well-oriented hexagonal wurtzite, with growth occurring in the c-direction. Figures 4.1 and 4.2 depict XRD scans typical of ZnO nanowires grown on an epitaxial layer of GaN deposited onto a <001> sapphire substrate. Figure 4.1 shows the results of a scan in which the angles between the x-ray detector and the incident beam, 2θ, and between the incident beam and the plane of the surface of the sample, Ω, are varied in synchronization. In this scan, the peak at 34.6° 2θ corresponds to the <0002> ZnO planes and the peak at 41.7° 2θ corresponds to the <006> Al_2O_3 planes, according to Bragg's Law with an x-ray wavelength of 1.54 Å. Figure 4.2 shows the results of a scan in which the 2θ angle is kept at a constant 34.6° while the Ω angle is varied. In this scan, the width of the peak represents the quality of the orientation of the <0002>

ZnO planes. The full-width half-max of this peak is 0.15° Ω, signifying that the c-planes of the ZnO nanowires are well aligned, and therefore the ZnO nanowires are well aligned. As stated previously, the x-ray diffractometer used was not equipped with a monochromator, hence the smaller secondary peak seen corresponding to ZnO in Figure 4.1.

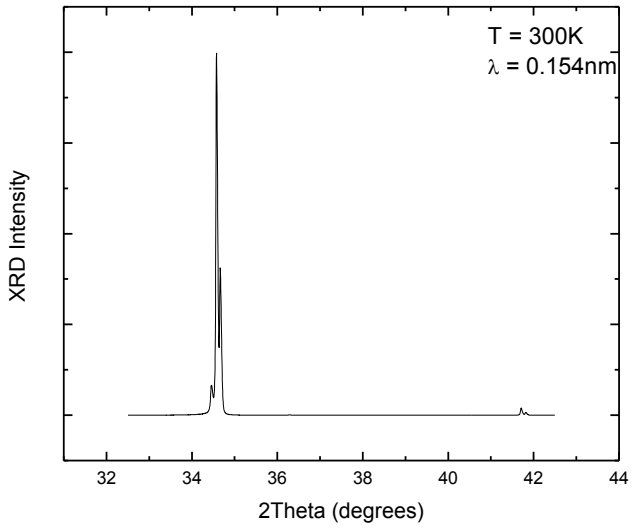

Figure 4.1 XRD 2θ-Ω of nanowires.
XRD 2θ-Ω scan depicting typical ZnO nanowire sample grown on a thin layer of GaN deposited onto a sapphire substrate.

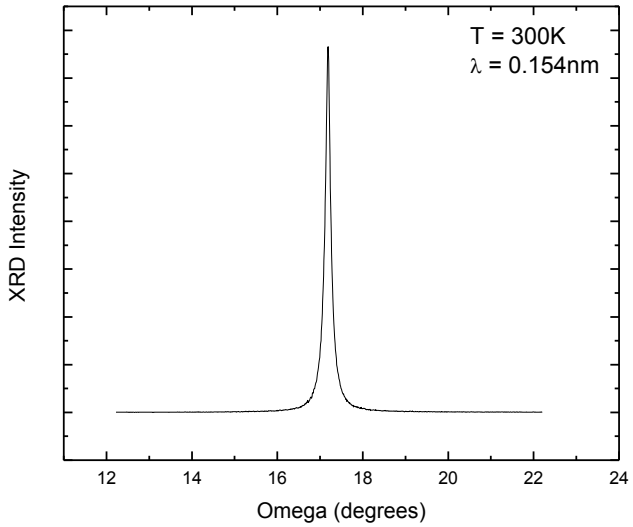

Figure 4.2 XRD Ω of nanowires.
XRD Ω scan depicting typical ZnO nanowire sample grown on a thin layer of GaN deposited onto a sapphire substrate. 2θ is held constant at 34.6°.

Figure 4.3 is an SEM image of typical ZnO nanowires. The wires were grown on an epitaxial layer of GaN without the use of any catalyst. The ZnO nanowires generally range from 20 μm down to less than a micron in length and 100-200 nm in diameter with a density on the order of 10^9 nanowires/cm^2. Due to the high absorption coefficients of the layers of the device structure, nanowires on the order of a single micron are preferred for device fabrication. Good alignment and orientation provide optimal electrical transport properties for the nanowires. This is essential as providing an efficient electron transport medium is one of the primary advantages of the nanowire scaffold. Simultaneously, a balance must be found between surface area and volume with respect to the diameter of the wire to maximize QD density while still maintaining good electrical conductivity. Pertaining to the orthogonal dimension, the nanowire length must be optimized to support the required device depth to maximize absorbed incident sunlight while minimizing free carrier drift distance.

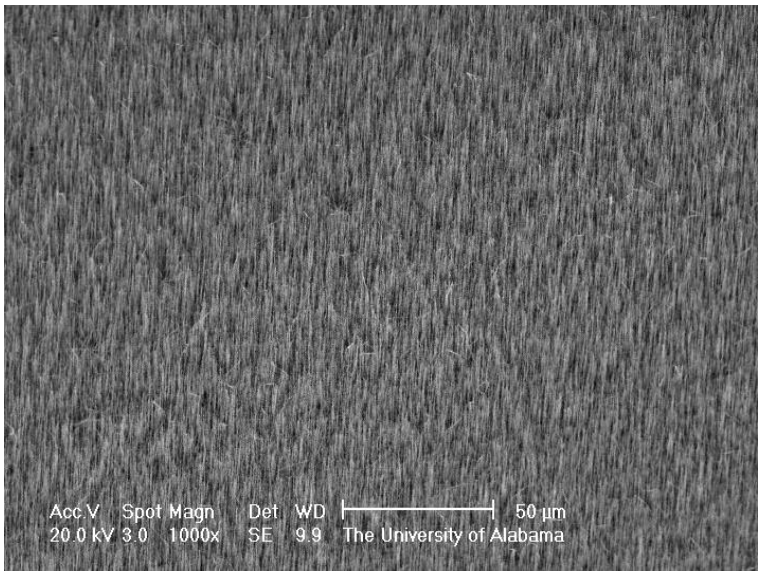

Figure 4.3 SEM of nanowires.
SEM image of typical ZnO nanowires grown via thermal CVD onto GaN thin film layer deposited onto <001> sapphire substrate. Nanowires are oriented in the c-direction.

Figure 4.4 is a confocal Raman spectroscopic scan of typical ZnO nanowires. A 532 nm laser was used to excite the sample. The spectrum is dominated by the E_2 phonon mode of wurtzite ZnO found at 438.9 cm^{-1}. The A^{LO} (longitudinal optical) peak at 577.7 cm^{-1} is an indicator of good alignment. The peak at 379.5 cm^{-1} corresponds to the A^{TO} phonon mode.

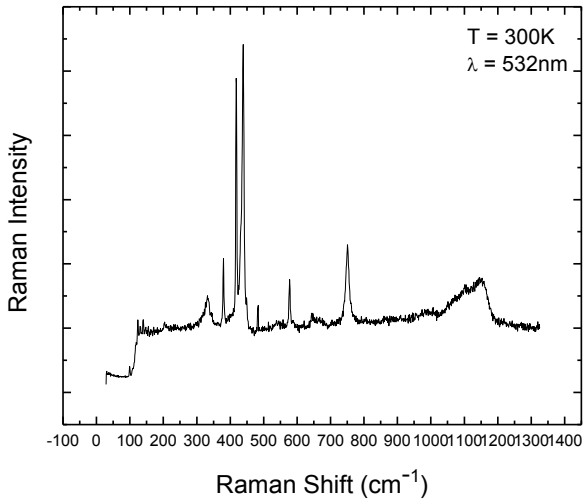

Figure 4.4 Raman of nanowires.
Confocal Raman spectroscopy scan of ZnO nanowires on sapphire substrate photoexcited by 532 nm laser.

Figure 4.5 depicts a confocal PL spectrum of typical ZnO nanowires. The sample was excited using a 266 nm laser source. The peak at 376 nm can be attributed to the ZnO; photon wavelengths of 376 nm correspond to energy of approximately 3.3 eV, approximately the band gap of ZnO. The defect, or green, peak at approximately 500 nm is nonexistent or very small in intensity compared to the ZnO band edge peak at 376 nm, further signifying well oriented nanowires with relatively low defect concentration.

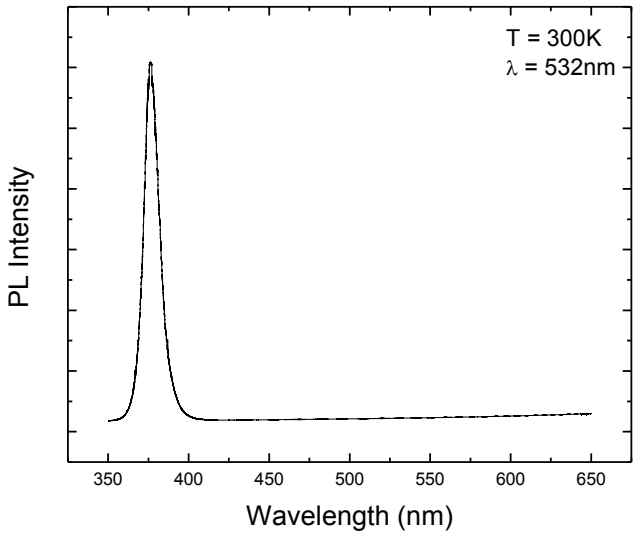

Figure 4.5 PL of nanowires.
Confocal PL spectroscopy scan of ZnO nanowires on sapphire substrate photoexcited by 266 nm laser.

Figure 4.6 shows a HRTEM image of a single ZnO nanowire grown using thermal CVD onto a <001> sapphire substrate, then scraped off the substrate and sonicated. The direction normal to the planes that can be identified in the image is the <0001> direction. This image verifies the alignment and orientation of the ZnO nanowires. The observed interplanar distance is in agreement with the expected value of c = 5.2 Å.

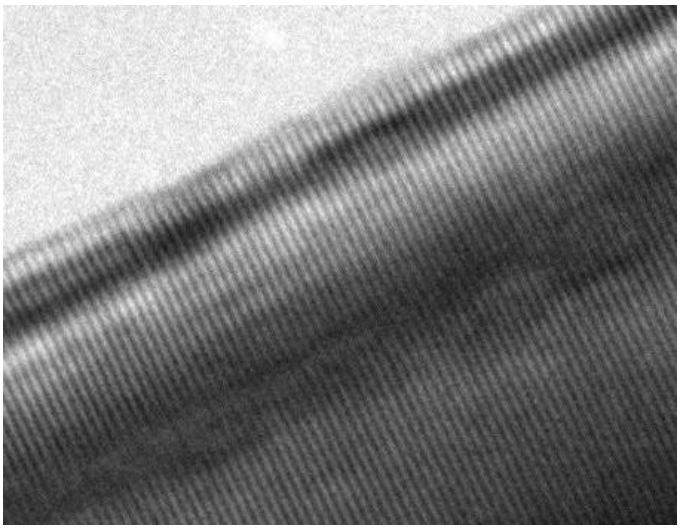

Figure 4.6 HRTEM of ZnO nanowire.
The growth direction is normal to the orientation of the distinguishable planes within the nanowire.

B. Ligand Exchange and Quantum Dot Attachment

In order to attach the InP-ZnS quantum dots to the ZnO nanowires, a ligand exchange was performed to replace the oleylamine ligand of the quantum dots with a MPA ligand. The chemical formula of oleylamine is $CH_3(CH_2)_7CH{=}CH(CH_2)_8NH_2$; the chemical formula of MPA is $HSCH_2CH_2COOH$. A not-to-scale, non-quantitatively representative graphical model of a quantum dot capped in oleylamine is shown in Illustration 4.1; a likewise graphical model of a quantum dot capped in MPA is shown in Illustration 4.2. It was expected that the shorter MPA ligand provides superior surface adhesion and interfacial electrical conductivity properties to oleylamine because of its thiol group and carboxylic acid tail. The basic methodology of the ligand exchange and quantum dot attachment is as follows. MPA was chosen as a linking molecule due to a thiol group on one end of the molecule and a carboxylic acid group on the other. The ligand exchange was performed in a solution of methanol. The relative number of methoxide ions of the methanol solution was increased; this was quantified in an approximate

manner by the use of pH test strips. Tetramethylammonium hydroxide was used for this purpose, as it pulled hydrogen atoms from methanol molecules. However, it would be preferable to find an alternate chemical for this purpose for further experimentation, as TMAOH is highly toxic. TMAOH and methoxide both pulled hydrogen atoms from the thiol groups of MPA. It was assumed this thiol group was then attracted to the ZnS shell of the quantum dots to form a disulfide bond. The other end of the MPA, the carboxylic acid tail, was assumed to be attracted to the surface of the ZnO nanowires to form an ester linkage.

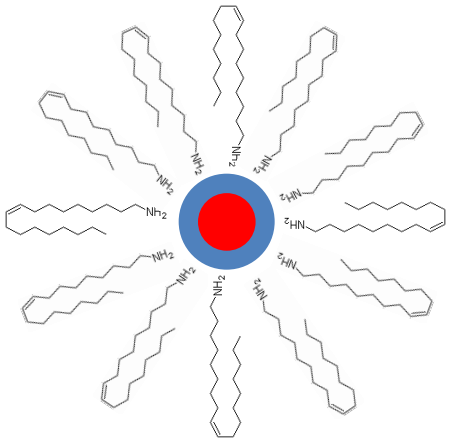

Illustration 4.1 Sketch of core-shell quantum dot capped in oleylamine ligand.

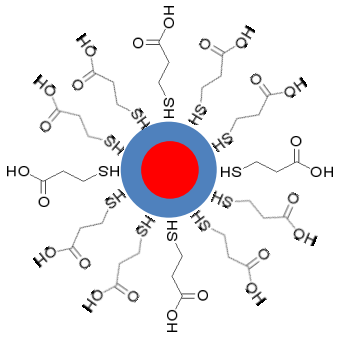

Illustration 4.2 Sketch of core-shell quantum dot capped in MPA ligand.

The ligand exchange procedure is based on a method designed and utilized by Leschkies, et al [4]. In the procedure detailed here and used for this project, quantum dots comprised of different materials are used with a different initial capping ligand from those in the initial procedure. The basic strategy of the ligand exchange remains the same, though portions and procedures have been altered. The ligand exchange procedure used is as follows: 30 mL methanol in 3-neck flask under N_2 purge through condenser in parallel with water-filled flask bubbler; allow to sit for ten minutes; introduce 0.4 mmol MPA, 0.043 g, to methanol in three-neck flask; using tetramethylammonium hydroxide, adjust methoxide ion concentration of solution to correspond to a reading of 12.0 on a pH strip; heat solution to 55°C in mineral oil bath for one hour while maintaining N_2 purge; introduce 4 mL of 5 mg/mL InP-ZnS core-shell quantum dots in toluene solution to the solution in the three-neck flask; while continuing N_2 purge, increase temperature of oil bath to 65° C and allow 20 hours for ligand exchange; remove flask from heated oil bath and allow to cool to room temperature; soak nanowire sample in solution 4 hours; remove sample from solution and blow dry under N_2. Unless otherwise noted, this is the procedure used throughout this research. A bulleted list of this procedure is included in the appendix. The following changes have been made from the initial ligand exchange

procedure: the N_2 purge flows through a condenser into three-neck flask in parallel with a flask of water set up as a bubbler; the methanol degassing under vacuum was completely replaced by simply allowing the methanol to sit in the three-neck flask at room temperature approximately ten minutes under the nitrogen purge; the introduction of 5mg/mL InP-ZnS core-shell quantum dots in toluene solution to the solution in the three-neck flask is doubled to 4 mL from 2 mL; the MPA was increased from 0.2 mmol to 0.4 mmol, 0.043 g, to match the increase in quantum dots; the pH of the solution was adjusted to 12.0, up from 11.4; ethyl acetate is no longer used to cause precipitation prior to soaking nanowires in solution. These changes were made in response to difficulties with the procedure stated in the cited paper. First, the methanol solution regularly evaporated, both during degas and the twenty hour ligand exchange. The purpose of the degassing was to attempt to remove as much water as possible from the methanol. The nitrogen purge also serves a similar purpose in removing the air, as well as any humidity in the air. Oxygen can act as a deterring agent in the ligand exchange process—under base conditions, oxygen will oxidize the MPA to the disulfide—and must be minimized in order to maximize the efficiency of the ligand exchange reaction. However, the evaporation of the methanol also contributes to another problem. By constantly reducing the amount of methanol in the flask, it becomes harder to control the amounts of other reagents that should be in the reaction to maximize efficiency. The goal of the reaction is for the quantum dots to completely shed the oleylamine ligand and to be completely coated in mercaptopropionic acid. The solution should then have enough mercaptopropionic acid to ensure complete coating of the quantum dots. Likewise, in order to maximize the potential for coating nanowires, the solution should be saturated in quantum dots. The concentration of the solution is 20 mg of quantum dots in approximately 35 mL of methanol solution; at the end of the 20 hour reaction period, slight

quantum dot precipitation is noticed after agitation. The optimal pH test strip reading of the solution, prior to quantum dot introduction was investigated, and found to be 12.0. A higher pH corresponds to a larger number of methoxide ions in the methanol solution. Methoxide is a strong base, which should pull hydrogen atoms from the mercaptopropionic acid in solution, encouraging the formation of a bond between the mercaptopropionic acid and the ZnS shell of the quantum dots. The high pH should also act as a catalyst in the formation of the bond between the ZnO and the mercaptopropionic acid. Lastly, the effect of ethyl acetate as a precipitating agent in the post-ligand exchange quantum dot in methanol solution on final nanowire coating was investigated and found to reduce attached quantum dot on nanowire concentration.

Using the ligand exchange procedure stated above, several samples were prepared for characterization. Samples prepared for characterization after ligand exchange were ZnO nanowires grown on sapphire substrate using thermal CVD with zinc acetate seed. Samples have been prepared using the stated procedure with 590 nm quantum dots, 650 nm quantum dots, and a combination of both 590 and 650 nm quantum dots. These samples have been characterized via confocal PL spectroscopy, confocal Raman spectroscopy, TEM EDS, and HRTEM. Figure 4.7 shows a combination of two confocal PL spectroscopic scans of a ZnO nanowire sample grown on a sapphire substrate. One scan was performed using a 266 nm laser as a photoexcitation source; the second scan was performed using a 532 nm laser. This was done to compare to the similar combination of scans depicted in Figure 4.8, performed on the same sample after the quantum dot attachment procedure had been performed. With 266 nm excitation, a photoluminescence peak was seen at ~390 nm as expected corresponding to the ZnO nanowires. Also as expected, for the bare nanowire sample depicted in Figure 4.7, no photoluminescence peak was observed under 532 nm excitation; ZnO did not seem to absorb the sub-bandgap

photoexcitation. However, for the nanowire sample sensitized with quantum dots, a peak was observed under 532 nm excitation. Quantum dots with a photoexcitation peak corresponding to 650 nm were used, and the new peak in Figure 4.8 corresponds to the band gap of the attached quantum dots. The appearance of a new photoluminescence peak corresponding to the photoemission spectra of the quantum dots verifies the presence and optical properties of the quantum dots after ligand exchange and attachment to the nanowire scaffold. The high intensity of the quantum dot peak is evidence of the excellent optical properties of the quantum dots. Once again, a 266 nm laser source and a 532 nm laser source were used for the individual scans that comprise the figure.

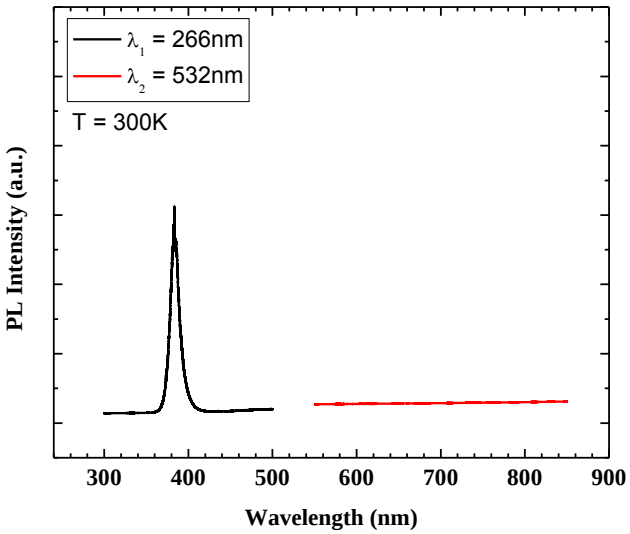

Figure 4.7 PL of as-grown nanowires.
Confocal PL spectroscopy scans of ZnO nanowires on sapphire substrate. Scan on left of graph was performed using a 266 nm laser excitation source; scan on right of graph was performed using a 532 nm laser excitation source.

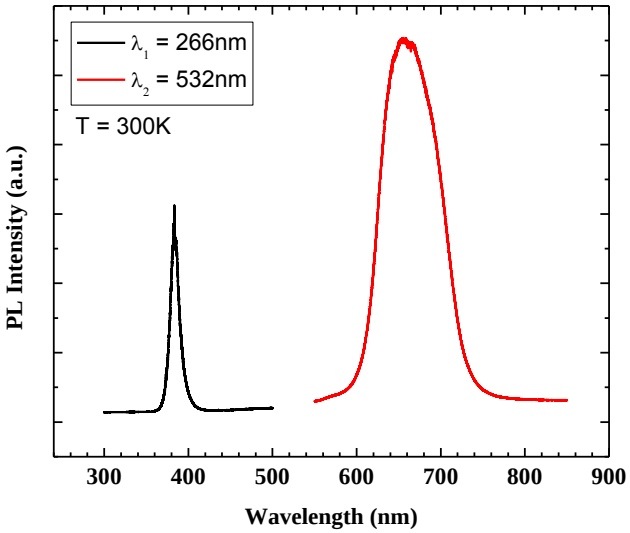

Figure 4.8 PL of quantum dot functionalized nanowires.
Confocal PL spectroscopy scans of 650 nm InP-ZnS core-shell quantum dot functionalized ZnO nanowires on sapphire substrate. Scan on left of graph was performed using a 266 nm laser excitation source; scan on right of graph was performed using a 532 nm laser excitation source. Standard stated ligand exchange and quantum dot attachment procedure was used.

Figure 4.9 depicts the normalized confocal PL spectra excited by a 532 nm laser of samples prepared using the updated procedure with 590 nm quantum dots, with 650 nm quantum dots and with both 590 and 650 nm quantum dots. Each curve of Figure 4.9 has been normalized to match peak intensity to emphasize spectral shape. It is currently believed that the higher energy peaks of the sample which includes both sizes of quantum dots are quenched by the lower energy peaks; as high energy photons are emitted, they are then captured by the lower energy quantum dots and re-emitted at a lower energy, with excess energy lost to lattice vibrations, etc. Figure 4.10 depicts the confocal Raman scan of a quantum dot functionalized nanowire sample on sapphire substrate excited by a 532 nm laser source. The phonon peak present at 306 cm^{-1} corresponds to a TO (Γ) Raman mode of InP [21, 22] seen earlier in Figure 3.3; the presence of this peak is further evidence of the presence and unaltered optical properties of the attached

quantum dots. The phonon peaks corresponding to the ZnO nanowires remain present at 379.5 cm^{-1}, 438.9 cm^{-1} and 577.7 cm^{-1}. 650 nm photoemission peak quantum dots were attached to the nanowire sample depicted in Figure 4.10.

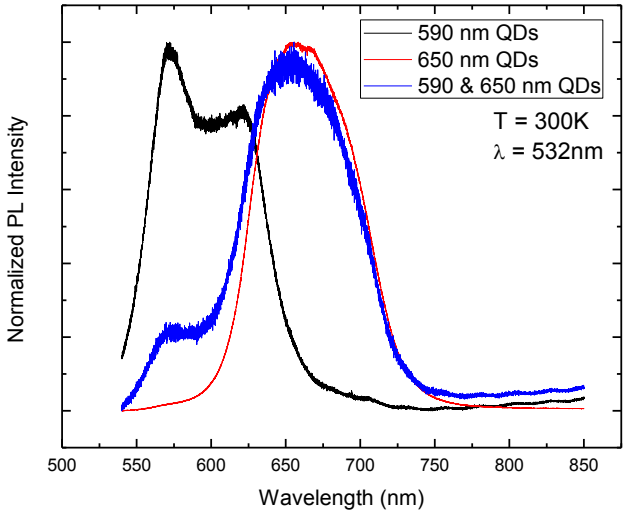

Figure 4.9 PL of various sized quantum dot functionalized nanowires.
Normalized confocal PL spectroscopy scan of expected 590, 650 and 590 & 650 nm photo-emission peak InP-ZnS quantum dot functionalized ZnO nanowires. A 532 nm laser excitation source was used. The standard stated ligand exchange and quantum dot attachment procedure was used.

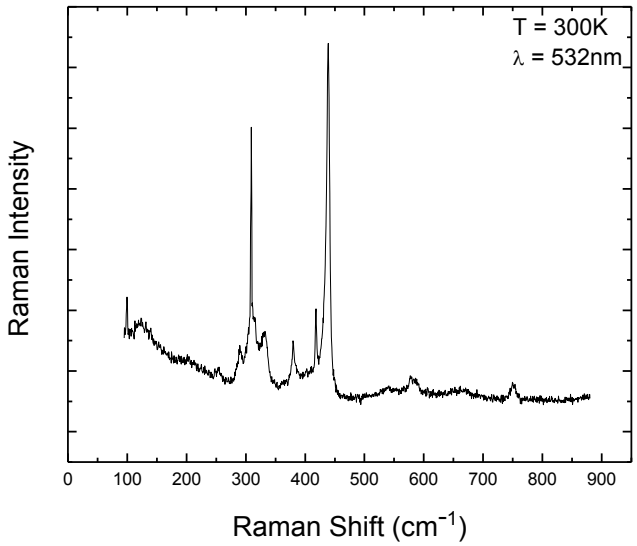

Figure 4.10 Raman of quantum dot functionalized nanowires.
Confocal Raman spectroscopy scan of InP-ZnS quantum dot functionalized ZnO nanowires on sapphire substrate. A 532 nm laser excitation source is used.

Figures 4.11 and 4.12 show TEM images of a ZnO nanowire with 650 nm InP-ZnS quantum dots attached. The ligand exchange and quantum dot attachment procedure described previously was used on a ZnO nanowire array grown on GaN thin film on sapphire substrate. The nanowire sample was removed from the substrate after quantum dot attachment. The sample was submerged in ethanol and sonicated. A dense monolayer of nanoparticles can be seen along the surface of the nanowire. Many of the nanoparticles can be verified as quantum dots via lattice matching. The interplanar distance visible in the nanoparticles corresponds to the expected value of 5.86 Å for InP lattice planes. Figure 4.11 features black circles highlighting such nanoparticles for which the planes are easily recognized, one of which being the focus of the inlaid image. Figure 4.12 features a nanowire from the same sample, with a white arrow indicating the direction of the c-plane, which is the direction of nanowire growth. As can be seen, the

monolayer of nanoparticles is dense both along the length and top of the nanowire, indicating that MPA-capped quantum dots adhere well both to a- and to c-plane surfaces of ZnO nanowires.

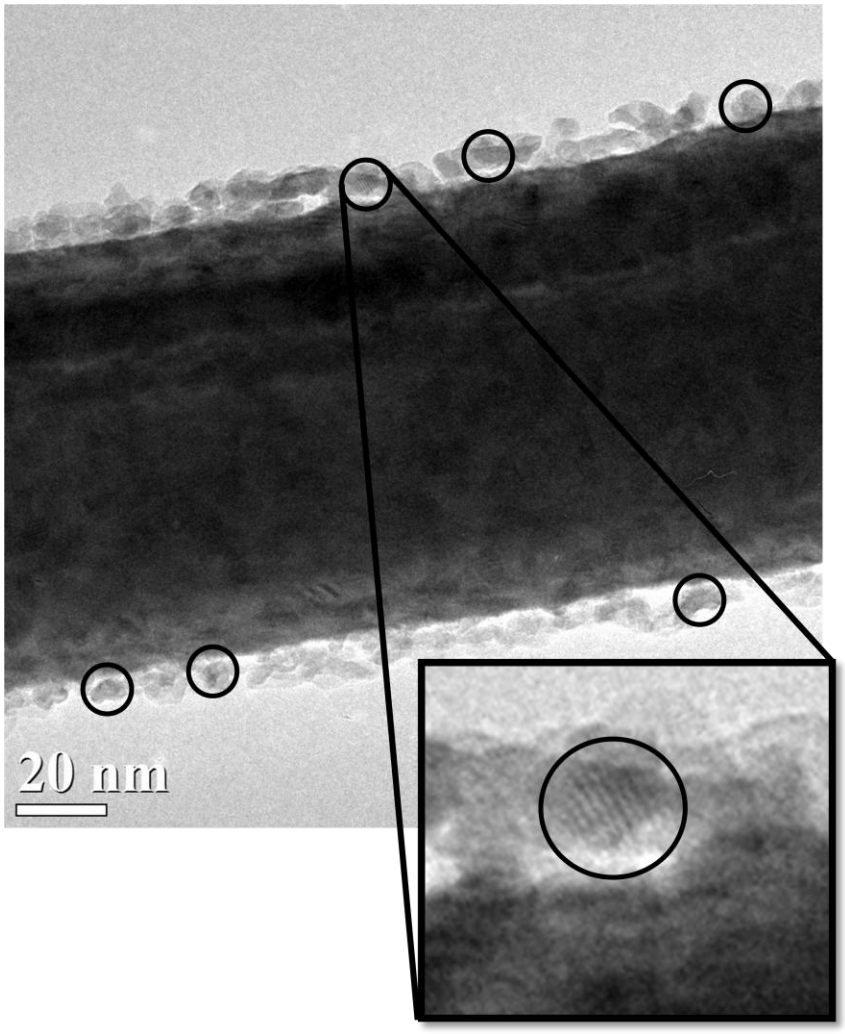

Figure 4.11 TEM of quantum dot functionalized nanowire.
TEM image of ZnO nanowire removed from nanowire array sample treated with quantum dot attachment procedure. Black circles added to indicate attached InP-ZnS quantum dots, verified via lattice matching. Inlay displays a subsection of image under greater zoom to emphasize visible InP lattice planes.

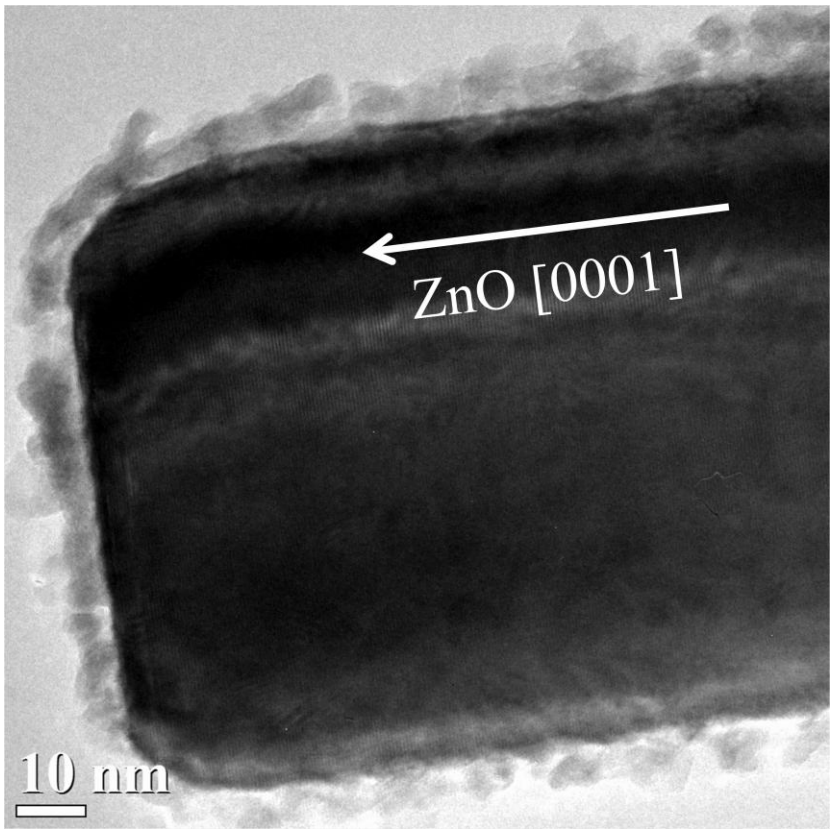

Figure 4.12 TEM of quantum dot functionalized nanowire.
TEM image of ZnO nanowire removed from nanowire array sample treated with quantum dot attachment procedure. White arrow and text "ZnO [0001]" added to indicate direction of growth during nanowire synthesis. Notice presence of quantum dots along both a- and c-plane surfaces of nanowire.

Figure 4.13 depicts an HRTEM image of a ZnO nanowire with 650 nm InP-ZnS nanoparticles attached. Ligand exchange and quantum dot attachment procedure was used on a ZnO nanowire array grown on sapphire substrate. The procedure varied from the procedure stated earlier, using half the suggested concentration of quantum dots and mercaptopropionic acid. Ligand exchange procedure was performed at pH test strip reading of approximately 11.3. The nanowire sample was removed from the substrate after quantum dot attachment. The sample was submerged in ethanol and sonicated. Either a single large quantum dot or a group of quantum dots can be seen attached to the surface of the nanowire. Lattice planes can be seen

within both the nanowire and the attached nanoparticle. The planes in the nanowire can be verified as corresponding to the lattice spacing of ZnO, while a portion of the planes in the nanoparticle can be verified as corresponding to the lattice spacing of InP.

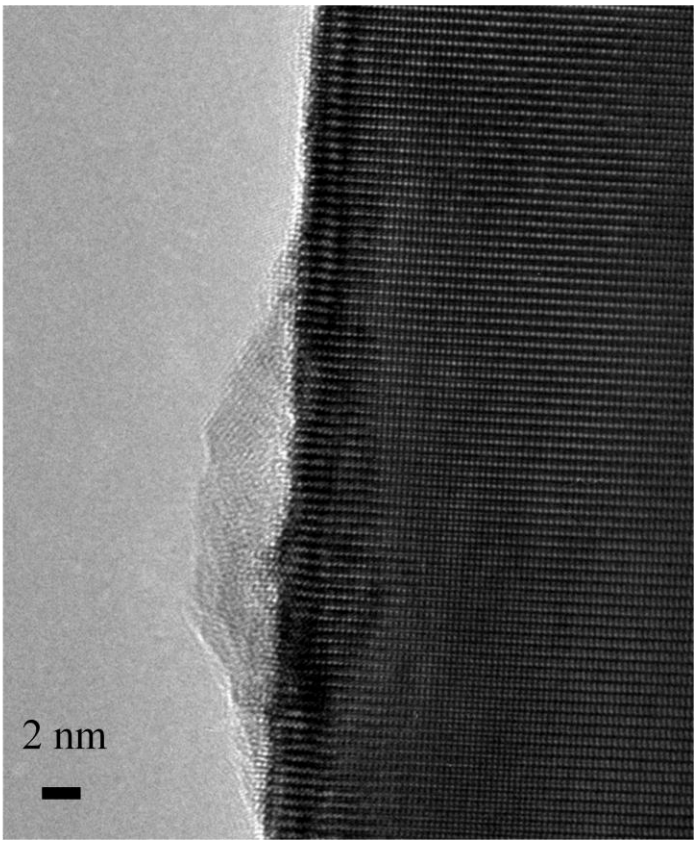

Figure 4.13 HRTEM of quantum dot functionalized nanowire.
HRTEM image of ZnO nanowire removed from nanowire array sample treated with quantum dot attachment procedure. Lattice planes can be seen in both nanowire, and in attached quantum dot. Black scale bar added manually, subsequent to image being captured.

Figure 4.14 depicts a STEM image of a ZnO nanowire with 650 nm InP-ZnS nanoparticles attached. The nanowire and attached nanoparticles correspond to the same sample and a similar nanowire and nanoparticle as that displayed in Figure 4.13. EDS imaging was performed on the nanowire, centered on the location of a nanoparticle. Concentrations of Indium, Phosphorus, and Sulfur can all be seen in the EDS mapping in the area of the nanoparticle. The

specific spatial presence of indium and phosphorus verifies the attached nanoparticle is comprised of quantum dots.

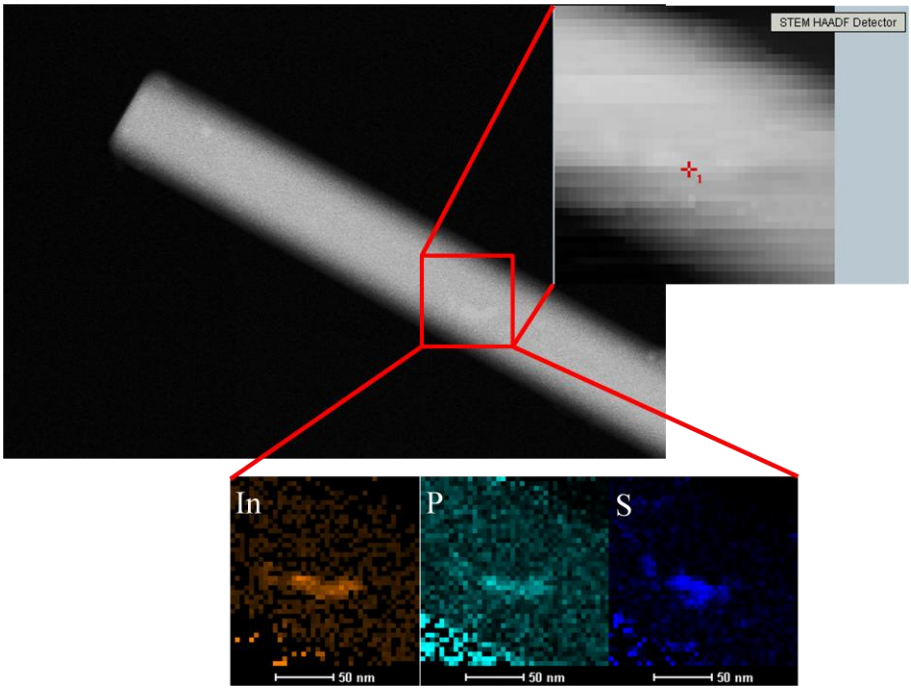

Figure 4.14 STEM and EDS of quantum dot functionalized nanowire.
STEM and EDS image of ZnO nanowire removed from nanowire array sample treated with quantum dot attachment procedure. EDS imaging centered on attached InP-ZnS quantum dot. Inlay depicts concentration of In, P, and S within EDS image. Brighter color corresponds to greater element concentration.

Figure 4.15 shows two UV-Vis transmission spectra. The red curve represents the transmission spectrum of quantum dot functionalized nanowires. The quantum dots attached to the nanowires have an emission peak at 590 nm. A corresponding trough can be seen at approximately 590 nm in the transmission spectrum. This shows the efficiency of quantum dots as a sensitizing absorption medium within photovoltaic architectures. Despite only forming a thin monolayer on the nanowires, the quantum dot sensitization layer absorbed efficiently enough to reduce near-band-gap photon transmission by approximately 75%. The black curve, included for comparison, represents the transmission spectrum of as-grown nanowires. This represents a prime utilization of the excellent optical properties of quantum dots.

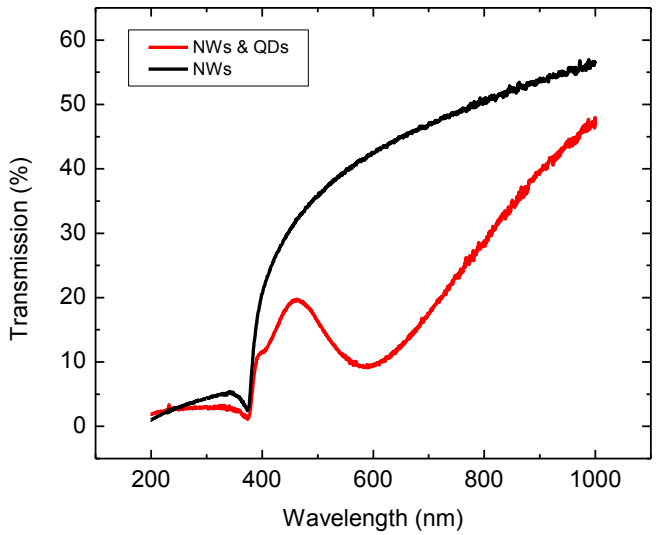

Figure 4.15 Transmission of quantum dot functionalized nanowires.
UV-Vis transmission spectroscopy scans comparing as-grown nanowires to quantum dot functionalized nanowires. The quantum dots attached to the nanowires have a 590 nm emission peak.

The last three figures of the ligand exchange and quantum dot attachment section use PL spectroscopy and the relative intensities of quantum dot peaks to determine the optimal parameters for the procedures. Figures 4.16 through 4.18 depict several of the quantum dot samples' confocal PL spectra organized by different properties. The spectra are presented in logarithmic scale. Intensity values are adjusted based on the ND filter that was used during each scan to account for varied intensities of light incident upon the samples throughout various scans. Figure 4.16 displays the spectra organized by the specific quantum dots attached to each sample: 526 nm, 590 nm, 590 nm, 650 nm, and both 590 and 650 nm. Figure 4.17 displays the spectra organized by use of ethyl acetate or no use of ethyl acetate to precipitate the quantum dots after the ligand exchange prior the quantum dot attachment to ZnO nanowire samples. It is shown to have little or no positive effect, with the trend showing less intensity generally when using ethyl

acetate. Lastly, Figure 4.18 shows the spectra organized by the pH test strip reading of the quantum dot ligand exchange and attachment solution prior to the addition of quantum dots. A pH test strip reading corresponding to 12.0 appears to be optimal to maximize quantum dot attachment as it corresponds to PL spectroscopy.

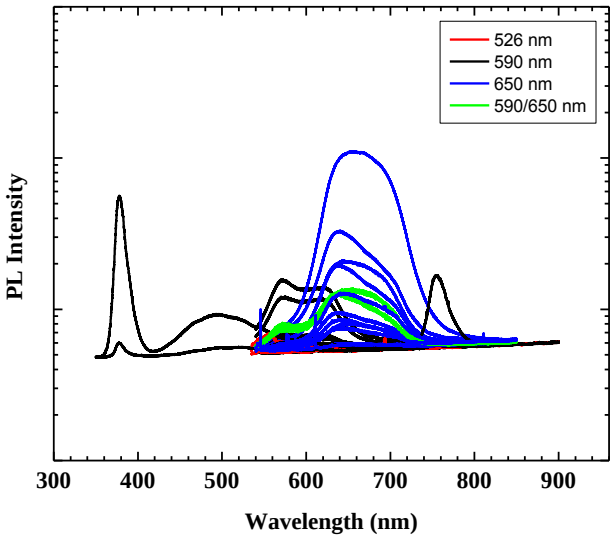

Figure 4.16 PL of various sized quantum dot functionalized nanowires.
Confocal PL spectroscopy scans of InP-ZnS quantum dot functionalized ZnO nanowire samples organized by the quantum dots used to functionalize the nanowires. Intensities have been adjusted only to compensate for ND filters. The peaks to the left of 510 nm and to the right of 710 nm correspond to the ZnO nanowires.

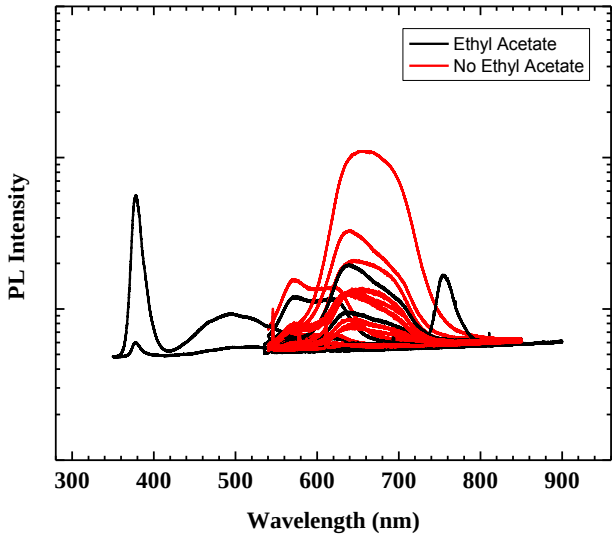

Figure 4.17 PL of forced- and non- precipitated quantum dot attachment.
Confocal PL spectroscopy scans of InP-ZnS quantum dot functionalized ZnO nanowire samples organized by the use or lack of use of ethyl acetate in the quantum dot attachment procedure. Intensities have been adjusted only to compensate for ND filters. The peaks to the left of 510 nm and to the right of 710 nm correspond to the ZnO nanowires.

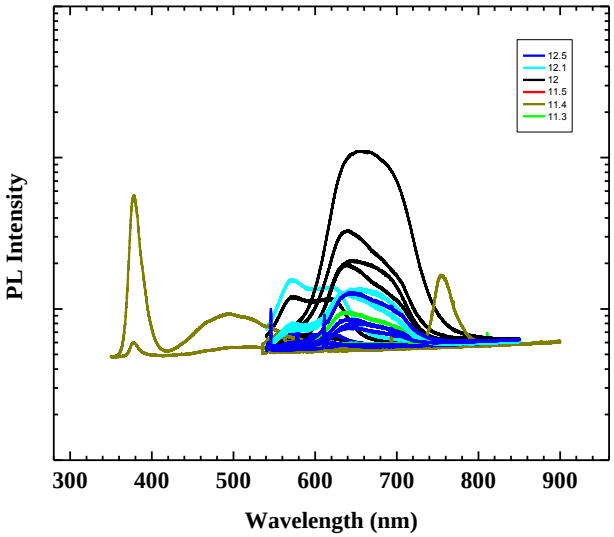

Figure 4.18 PL of various acidity solution quantum dot attachment.
Confocal PL spectroscopy scans of InP-ZnS quantum dot functionalized ZnO nanowire samples organized by the pH test strip reading of the quantum dot ligand exchange and attachment solution prior to the introduction of quantum dots. Intensities have been adjusted only to compensate for ND filters. The peaks to the left of 510 nm and to the right of 710 nm correspond to the ZnO nanowires.

C. Poly(3-hexylthiophene) Deposition

P3HT is deposited in a trichlorobenzene solution at 70° C via drop coating method. Several magnetized holders have been devised to allow selective placement of P3HT. Holders make use of O-rings to make a seal through which P3HT will not flow to undesired areas of samples; unfortunately, capillary action due to nanowires can still present difficulties. The design of the holders is included in the appendix for reference. Trichlorobenzene is allowed to dry under vacuum. After sufficient thickness has been deposited, P3HT is annealed under vacuum at 200° C for two hours. Due to the efficiency of drop coating while in solution of trichlorobenzene, P3HT thoroughly fills within the nanowire scaffold and has excellent electrical and optical properties after annealing. Figures 4.19 and 4.20 show SEM images of cross

sectional views of P3HT deposited onto nanowires. Figure 4.19 shows P3HT filling the entire cross section of the nanowire array with poorly-aligned long nanowires. Figure 4.20 shows thorough infiltration into a highly dense nanowire array, with very few gaps and cavities. The distances measured and depicted in Figure 4.20 were added to the image using SEM control software. The even-texture of the plane of P3HT is also evident in Figure 4.20; this is important to maintain optimized required free carrier drift distance. The sample in Figure 4.19 has not been annealed; the sample in Figure 4.20 has been annealed.

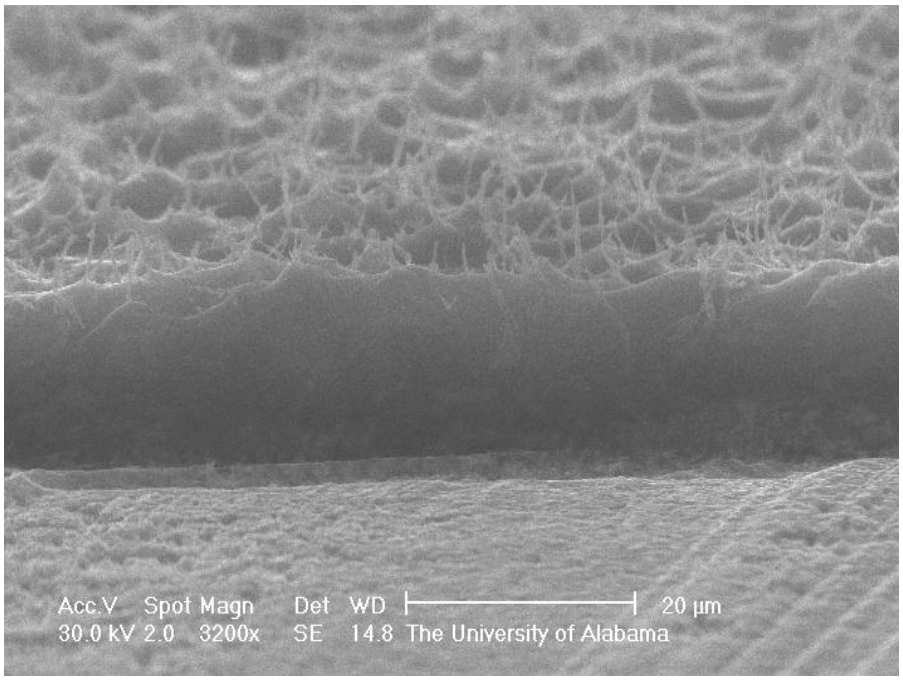

Figure 4.19 SEM of non-annealed P3HT matrix in nanowire scaffold.
Cross-sectional SEM image of drop coated P3HT matrix embedded into an array of ZnO nanowires on sapphire substrate. Section of P3HT and nanowires has been scraped away using a razor blade to expose the inner matrix for cross-sectional view.

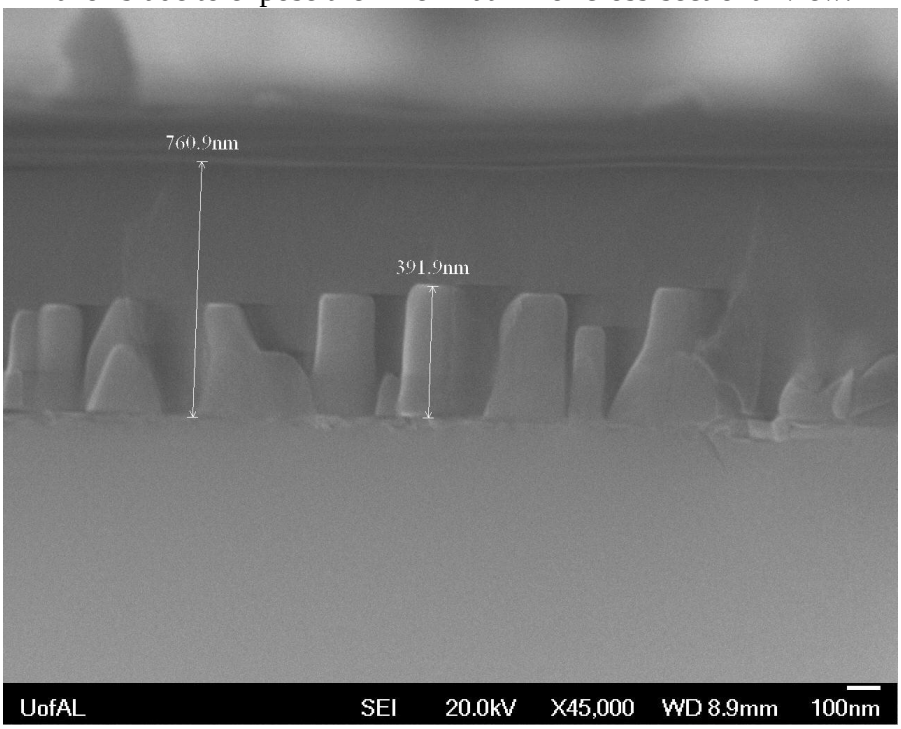

Figure 4.20 SEM of annealed P3HT matrix in nanowire scaffold.
Cross-sectional SEM image of drop coated and annealed P3HT matrix embedding an array of ZnO nanowires on sapphire substrate. Section of substrate, P3HT, and nanowires has been scraped away using a razor blade to expose the inner matrix for cross-section view.

Some of the primary disadvantages of P3HT are its resistivity and poor electron and hole mobilities. Annealing is one procedure that has been shown to improve these characteristics, particularly those of regio-regular P3HT. Several temperatures and conditions were attempted to find an optimized annealing procedure. Results had a relatively large variance from sample to sample; however, a 2 hour anneal in vacuum in a tube furnace set to 200° C seemed to regularly provide the best results. Figure 4.21 shows current-voltage characteristics under illumination for a P3HT on an n-doped GaN thin-film on sapphire sample both before and after annealing. As can be seen, an approximately half-order of magnitude increase can be seen in conductivity after annealing. Eutectic was required to prevent a Schottky effect between probe and GaN, however, the p-n junction effect of the P3HT on the n-doped GaN thin-film was as expected. The higher current associated with the annealed sample at higher magnitude voltages corresponds to a higher conductivity.

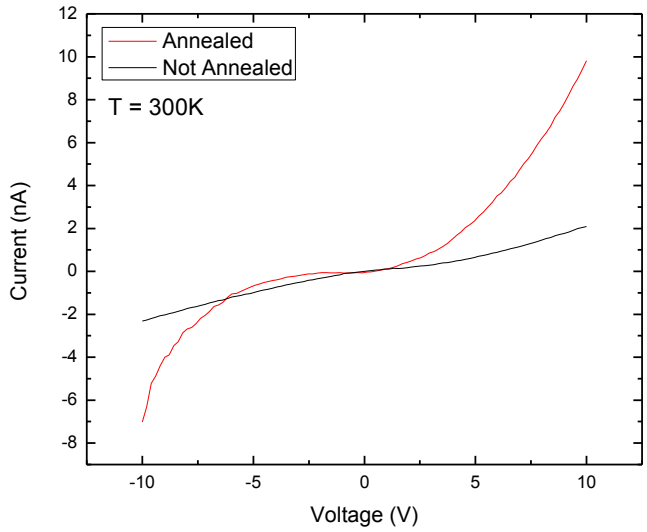

Figure 4.21 IV of P3HT on GaN.
Device IV curves of a device sample of P3HT deposited onto an n-doped GaN thin-film coated onto a sapphire substrate. IV curves were taken prior to and following annealing.

Experiments with plasma etching were attempted to planarize the top surface of P3HT, in order to optimize the interface between P3HT and deposited contacts; however, insufficient data was completed to report conclusively. Plasma etch planarization remains a potential viable tool for providing a more uniform back plane for Au contacts, to minimize required hole transport distance. The Au deposition is performed using a BioRad Gold Sputter Coater. For the deposition, a voltage of approximately 2kV with a current of 25mA is used with the sample being held at a pressure of approximately 10^{-4} bar.

CHAPTER 5

DEVICE

The advantages offered by the combination of materials and structures utilized throughout the design and fabrication of the device may be largely illustrated via three measurements. One of the most surprising and useful phenomena seen may be observed using PL spectroscopy. When P3HT is with a quantum dot functionalized nanowire array, the PL peaks lose intensity compared to a non-functionalized nanowire array. Figure 5.1 shows the PL spectra of the architecture as each element is added. The plain nanowires had no PL peak corresponding to 532 nm excitation. However, the quantum dots and the P3HT both absorbed the 532 nm laser excitation, with peaks observed at approximately 650 nm corresponding to quantum dots and approximately 630 nm and 710 nm corresponding to P3HT absorption and emission. The photoluminescence peak of quantum dots and the overlapping photoluminescence peak of P3HT are both more intense than the corresponding photoluminescence peak of P3HT with embedded quantum dots. This suggests that radiative recombination is actually reduced within the device by the overlapping absorption spectra and energy levels of P3HT and the quantum dots. This is a similar effect to that noticed in study done with P3HT and an ITO interface with injected charge carriers provided by poly(4-vinylphenol) [29], as well as a study done with P3HT with embedded carbon nanotubes [30]. This apparent PL quenching is actually a very positive effect

for ultimate device performance as an optimized solar cell seeks to minimize the loss of energy through radiative recombination.

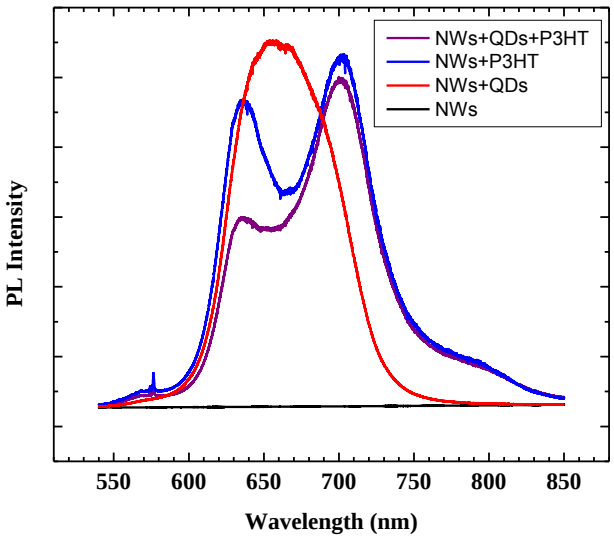

Figure 5.1 PL of device and device structural elements.
Confocal PL spectroscopy scans of various stages of device integration. All scans taken using 532 nm laser excitation source and approximately equal illumination intensity and filtering. Notice the reduced intensity of the photoluminescence peaks at approximately 630 nm and 650 nm when quantum dots and P3HT are utilized within the same device structure. Spectra are not normalized.

The effectiveness of quantum dots as an absorption medium within such a device structure may be seen with UV-Vis absorption and transmission spectroscopy. Figure 5.2 shows the UV-vis transmission spectra of the architecture as each element is added. The quantum dots utilized in Figure 5.2 are tuned to a band gap of 590 nm; however, despite the relatively low wavelength seen here, quantum dots are nonetheless shown to be an effective option for extending the absorption range of hybrid solar cells into the infrared spectrum. The spectra cover the solar spectrum well, with ZnO efficiently absorbing around 3.3-3.4 eV, P3HT absorbing as low as 2.0 to 1.6 eV, and quantum dots tunable via size to efficiently harvest from between the absorption spectra of ZnO and P3HT even into the infrared range. As the thickness of the device

increases, the transmission percentage in the range outside the efficient absorption wavelength range decreases, likely due to scattering.

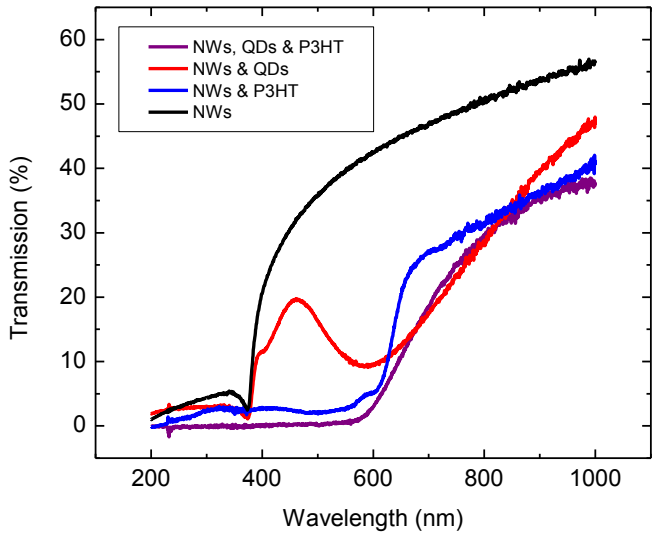

Figure 5.2 Transmission of device and device structural elements.
UV-Vis transmission spectroscopy scans of various stages of device integration. The quantum dots used in both quantum dot functionalized samples have a 590 nm emission peak.

Ultimately, the effect of any design decision for photovoltaics must be spearheaded by an improvement in efficiency. Electrical measurements show the effect of implementing a quantum dot absorption layer into the hybrid device structure. Figure 5.3 depicts device IV curves for two samples. The two samples were fabricated as well-aligned ZnO nanowire arrays on ZnAlO substrates. 650 nm quantum dots were then attached to one of the samples. P3HT was drop coated onto the center of both samples, leaving the corners to be probed. Lastly, the P3HT was annealed. As can be seen, both samples have differently shaped IV curves. However, both samples also respond to light by increasing free carriers, resulting in less impedance, representing p-n junctions, and producing a small photovoltage. Curves with lights off are compared to the curves taken with the lights on of the same sample. The curve of the quantum

dot sensitized sample shifts considerably further upon illumination, producing a photovoltage of approximately 0.75 V. This is evidence of the improved power efficiency of the quantum dot sensitized sample. Illustration 5.1 depicts a sketch of the electrical measurement probe scheme: the positive bias probe was placed on the gold contacts sputtered onto the P3HT matrix; the negative bias probe was placed on the ZnAlO thin film coating on the substrate.

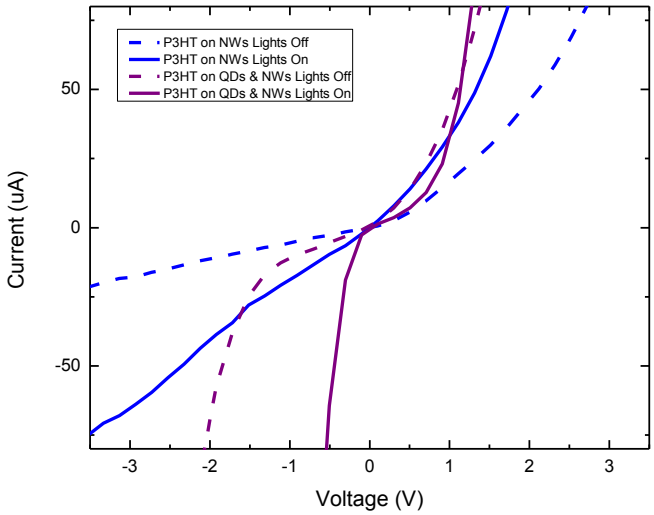

Figure 5.3 IV of device and device structural elements.
Device IV curves of a device sample with quantum dots and a device sample without quantum dots. Device IV curves are shown both under illumination and in dark.

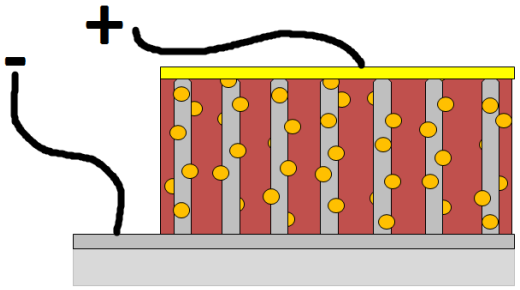

Illustration 5.1 Sketch of device electrical measurement schematic.

CHAPTER 6

CONCLUSION

A nanostructured, hybrid photovoltaic device architecture has been described. Processes for fabrication and characterization have been designed and tested. ZnO nanowires are grown on transparent, conducting substrates via thermal CVD, and characterized via PL spectroscopy, Raman spectroscopy, SEM, and TEM. A quantum dot ligand exchange and attachment procedure has been defined and optimized. Quantum dot attachment is characterized via PL spectroscopy, Raman spectroscopy, TEM, and EDS. An effective method of drop coating and annealing a P3HT polymer matrix to thoroughly fill a dense nanowire array has been designed and optimized. Complete device performance has been evaluated via PL spectroscopy, UV-Vis spectroscopy, and electrical measurements. This device architecture has been shown to offer several key benefits. The actual architecture makes use of structures that would work well with many different materials and fabrication techniques. For instance, if the fabrication procedures were changed to use a solution-growth method for the nanowires, the entire device could be produced without exceeding processing temperatures of 200° C. Also, the capability of using a dense monolayer of quantum dots as an absorbing layer not only opens up the possibility to selectively target specific regions of the solar spectrum, but also allows for the strategic placement of the primary absorption medium largely within a prime position for effective exciton disassociation and free carrier transport. The nanowire array maximizes surface area, specifically important for a thin quantum dot monolayer, for absorption mediums while still allowing for efficient free carrier transport pathways. A polymer hole-transport matrix allows for simple, effective deposition such as the drop coat method, and a non-caustic environment for

quantum dots. This is particularly important due to the capability to sensitize nanowire scaffolds with a dense quantum dot monolayer. P3HT specifically offers the advantage of being an excellent hole-trap medium, integral to minimize undesirable recombination avenues, as was seen in the photoluminescence quenching of the paired quantum dots and P3HT. The fabrication and characterization of a high-efficiency, low-cost hybrid nanostructured photovoltaic architecture has been demonstrated.

REFERENCES

[1] S.-H. Lee, *et al.*, "Al-Doped ZnO Thin Film: A New Transparent Conducting Layer for ZnO Nanowire-Based Dye-Sensitized Solar Cells," *The Journal of Physical Chemistry C,* vol. 114, pp. 7185-7189, 2010.

[2] H. Bi and R. R. LaPierre, "A GaAs nanowire/P3HT hybrid photovoltaic device," *Nanotechnology,* vol. 20, p. 465205, 2009.

[3] H. M. Chen, *et al.*, "Quantum Dot Monolayer Sensitized ZnO Nanowire-Array Photoelectrodes: True Efficiency for Water Splitting," *Angewandte Chemie International Edition,* vol. 49, pp. 5966-5969, 2010.

[4] K. S. Leschkies, *et al.*, "Photosensitization of ZnO Nanowires with CdSe Quantum Dots for Photovoltaic Devices," *Nano Letters,* vol. 7, pp. 1793-1798, 2007.

[5] R. D. Schaller and V. I. Klimov, "High Efficiency Carrier Multiplication in PbSe Nanocrystals: Implications for Solar Energy Conversion," *Physical Review Letters,* vol. 92, p. 186601, 2004.

[6] R. J. Ellingson, *et al.*, "Highly Efficient Multiple Exciton Generation in Colloidal PbSe and PbS Quantum Dots," *Nano Letters,* vol. 5, pp. 865-871, 2005.

[7] J. E. Murphy, *et al.*, "PbTe Colloidal Nanocrystals: Synthesis, Characterization, and Multiple Exciton Generation," *Journal of the American Chemical Society,* vol. 128, pp. 3241-3247, 2006.

[8] A. J. Nozik, "Quantum dot solar cells," *Physica E: Low-dimensional Systems and Nanostructures,* vol. 14, pp. 115-120, 2002.

[9] H. Yang and P. H. Holloway, "Enhanced photoluminescence from CdS:Mn/ZnS core/shell quantum dots," *Applied Physics Letters,* vol. 82, pp. 1965-1967, 2003.

[10] W. Shockley and H. J. Queisser, "Detailed Balance Limit of Efficiency of p-n Junction Solar Cells," *Journal of Applied Physics,* vol. 32, pp. 510-519, 1961.

[11] P. V. Kamat, "Quantum Dot Solar Cells. Semiconductor Nanocrystals as Light Harvesters†," *The Journal of Physical Chemistry C,* vol. 112, pp. 18737-18753, 2008.

[12] J. Blackburn, *et al.*, "Electron and hole transfer from indium phosphide quantum dots," *The Journal of Physical Chemistry B,* vol. 109, pp. 2625-2631, 2005.

[13] W. U. Huynh, *et al.*, "Hybrid nanorod-polymer solar cells," *Science,* vol. 295, pp. 2425-2427, 2002.

[14] T. W. Zeng, *et al.*, "Hybrid poly (3-hexylthiophene)/titanium dioxide nanorods material for solar cell applications," *Solar Energy Materials and Solar Cells,* vol. 93, pp. 952-957, 2009.

[15] T. Homma, *et al.*, "Interstitial pneumonia developed in a worker dealing with particles containing indium-tin oxide," *Journal of Occupational Health,* vol. 45, pp. 137-139, 2003.

[16] T. Pons, *et al.*, "Cadmium-free CuInS2/ZnS quantum dots for sentinel lymph node imaging with reduced toxicity," *Acs Nano,* vol. 4, pp. 2531-2538, 2010.

[17] K. Oda, "Toxicity of a low level of indium phosphide (InP) in rats after intratracheal instillation," *Industrial health,* vol. 35, pp. 61-68, 1997.

[18] A. TANAKA, *et al.*, "Pulmonary Toxicity of Indium-Tin Oxide and Indium Phosphide after Intratracheal Instillations into the Lung of Hamsters," *Journal of Occupational Health,* vol. 44, pp. 99-102, 2002.

[19] Y. Y. Lin, *et al.*, "Nanostructured metal oxide/conjugated polymer hybrid solar cells by low temperature solution processes," *J. Mater. Chem.,* vol. 17, pp. 4571-4576, 2007.

[20] D. C. Look, *et al.*, "Electrical properties of bulk ZnO," *Solid State Communications,* vol. 105, pp. 399-401, 1998.

[21] E. Bedel and et al., "Raman investigation of the InP lattice dynamics," *Journal of Physics C: Solid State Physics,* vol. 19, p. 1471, 1986.

[22] M. J. Seong, *et al.*, "Size-dependent Raman study of InP quantum dots," *Applied Physics Letters,* vol. 82, p. 185, 2003.

[23] J. Obrzut and K. A. Page, "Electrical conductivity and relaxation in poly(3-hexylthiophene)," *Physical Review B,* vol. 80, p. 195211, 2009.

[24] J. A. Hauch, *et al.*, "Flexible organic P3HT: PCBM bulk-heterojunction modules with more than 1 year outdoor lifetime," *Solar Energy Materials and Solar Cells,* vol. 92, pp. 727-731, 2008.

[25] K. Kumari, *et al.*, "Effect of CdSe quantum dots on hole transport in poly(3-hexylthiophene) thin films," *Applied Physics Letters,* vol. 92, p. 263504, 2008.

[26] K. Kusum and et al., "Enhancement in hole current density on polarization in poly(3-hexylthiophene):cadmium selenide quantum dot nanocomposite thin films," *Applied Physics Letters,* vol. 94, p. 213503, 2009.

[27] D. H. Kim, *et al.*, "Significant enhancement of the power conversion efficiency for organic photovoltaic cells due to a P3HT pillar layer containing ZnSe quantum dots," *Optics Express,* vol. 20, pp. 10476-10483, 2012.

[28] K. M. Coakley and M. D. McGehee, "Conjugated Polymer Photovoltaic Cells," *Chemistry of Materials,* vol. 16, pp. 4533-4542, 2004/11/01 2004.

[29] V. Singh, *et al.*, "Evidence of photoluminescence quenching in poly(3-hexylthiophene-2,5-diyl) due to injected charge carriers," *Synthetic Metals,* vol. 158, pp. 283-286, 2008.

[30] P. J. Goutam, *et al.*, "Photoluminescence Quenching of Poly(3-hexylthiophene) by Carbon Nanotubes," *The Journal of Physical Chemistry C,* vol. 116, pp. 8196-8201, 2012/04/12 2012.

APPENDIX

Ligand Exchange and Quantum Dot Attachment Procedure:

- Pour 30 mL methanol into a 3-neck flask under the flow of N_2 through a condenser and water-filled flask bubbler.
- Allow to purge for 10 minutes.
- Add 0.4 mmol MPA (0.043 g) to the 3-neck flask.
- Add chemical to ionize methanol molecules into methoxide ions; TMAOH was used, preferably use something less toxic. Using a clean pipette, deposit a drop of methanol solution onto a pH test strip. Continue to do this until the color of the pH test strip corresponds to a pH of 12.0.
- Heat the solution to 55° C for one hour using a mineral oil bath.
- Add 4 mL of 5 mg/mL InP-ZnS core-shell quantum dots in toluene solution to the 3-neck flask.
- Increase the temperature of the oil bath to 65° C and allow 20 hours for the ligand exchange. Cover the 3-neck flask with an opaque material to prevent illumination of the solution.
- Remove the 3-neck flask from the oil bath and allow the solution to cool to room temperature. The N_2 purge can be removed after the solution has cooled.
- Shake the solution, then allow a nanowire sample to soak in the solution for 4 hours.
- Remove the sample from the solution and blow dry under N_2.

Vials of InP-ZnS core-shell quantum dots in solution of toluene purchased from NN-Labs. All three vials contain the same materials; however, based on the quantum dot size, the coloration of the solution changes.

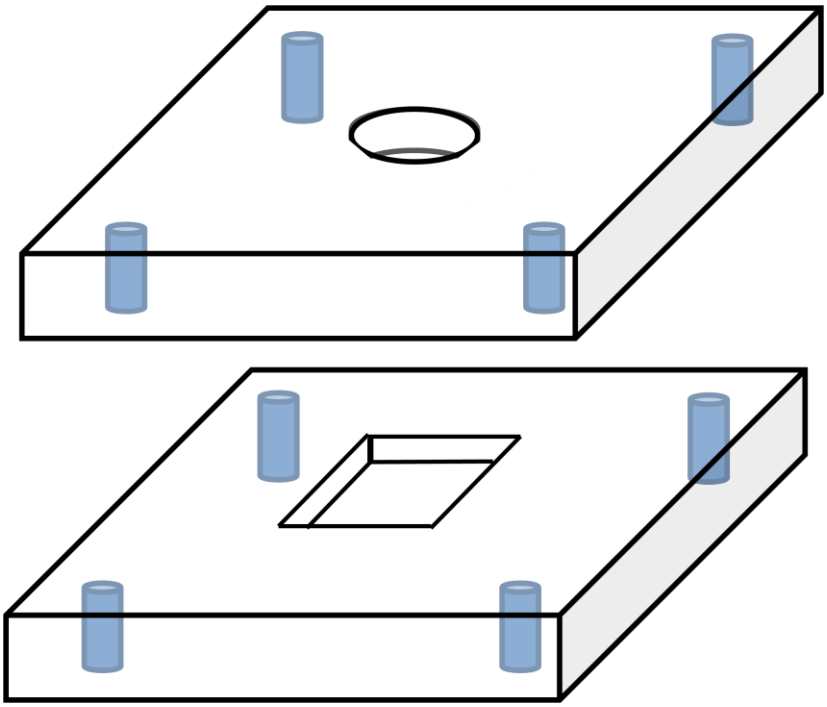

Teflon holder designed to selectively deposit P3HT onto samples for electrical measurement probing onto substrate. Light blue cylinders represent magnets. Clips used to hold holder and sample in place with viton o-ring used to create seal on sample surface.